

Inactivation of PP2A by a recurrent mutation drives resistance to MEK inhibitors

Authors: Caitlin M. O'Connor¹, Daniel Leonard², Danica Wiredja³, Rita A. Avelar⁴, Zhizhi Wang⁵, Daniela Schlatzer³, Benjamin Bryson⁶, Eesha Tokala⁶, Sarah E. Taylor², Aditya Upadhyay⁶, Jaya Sangodkar⁷, Anne-Claude Gingras⁸, Jukka Westermarck⁹, Wenqing Xu⁵, Analisa DiFeo⁴, David L. Brautigan¹⁰, Shozeb Haider¹¹, Mark Jackson⁶, Goutham Narla^{7, *}.

Affiliations:

¹Department of Pharmacology, Case Western Reserve University, Cleveland, OH, USA.

²Department of Pathology, Case Western Reserve University, Cleveland, OH, USA.

³Department of Proteomics and Bioinformatics, Case Western Reserve University, Cleveland, OH, USA.

⁴Department of Pathology, University of Michigan, Ann Arbor, MI, USA.

⁵Department of Biological Structure, University of Washington, Seattle, WA, USA.

⁶Case Comprehensive Cancer Center, Case Western Reserve University, Cleveland, OH, USA.

⁷ Department of Internal Medicine: Genetic Medicine, University of Michigan, Ann Arbor, MI, USA.

⁸Lunenfeld-Tanenbaum Research Institute, Sinai Health System, Toronto, ON, Canada; Department of Molecular Genetics, University of Toronto, Toronto, ON, Canada.

⁹Turku Centre for Biotechnology, University of Turku and Åbo Akademi University, Turku, Finland.

¹⁰Department of Microbiology, Immunology, and Cancer Biology, University of Virginia, Charlottesville, VA, USA

¹¹Department of Pharmaceutical and Biological Chemistry, University College London, London, United Kingdom

Keywords: PP2A, PPP2R1A, RAS, AZD-6244, drug resistance

Additional Information:

To whom correspondence should be addressed:

Goutham Narla, email: gnarla@med.umich.edu

Conflict of Interest Statement: The authors declare no potential conflicts of interest.

Number of Figures: 5

1 **Abstract**

2 The serine/threonine Protein Phosphatase 2A (PP2A) functions as a tumor suppressor by
3 negatively regulating multiple oncogenic signaling pathways. The canonical PP2A holoenzyme is
4 comprised of a scaffolding subunit (PP2A A α / β), which serves as the platform for binding of both
5 the catalytic C subunit and one regulatory B subunit. Somatic heterozygous missense mutations in
6 *PPP2R1A*, the gene encoding the PP2A A α scaffolding subunit, have been identified across
7 multiple cancer types, but the effects of the most commonly mutated residue, Arg-183, on PP2A
8 function have yet to be fully elucidated. In this study, we used a series of cellular and *in vivo*
9 models and discovered that the most frequent A α R183W mutation formed alternative
10 holoenzymes by binding of different PP2A regulatory subunits compared to wild type A α ,
11 suggesting a rededication of PP2A functions. Unlike wild type A α , which suppressed
12 tumorigenesis, the R183W mutant failed to suppress tumor growth *in vivo* through activation of
13 the MAPK pathway in RAS-mutant transformed cells. Furthermore, cells expressing R183W were
14 less sensitive to MEK inhibitors. Taken together, our results demonstrate that the R183W mutation
15 in PP2A A α scaffold abrogates the tumor suppressive actions of PP2A, thereby potentiating
16 oncogenic signaling and reducing drug sensitivity of RAS-mutant cells.

17

18

19

20

21

22

1 **Introduction**

2 The serine/threonine Protein Phosphatase 2A (PP2A) functions as a tumor suppressor by
3 negatively regulating multiple oncogenic signaling pathways, particularly RAS driven signaling^{1,2}.
4 Importantly, PP2A inactivation is necessary to fully transform RAS expressing human epithelial
5 cells, and PP2A and RAS have been shown to regulate overlapping signaling pathways,
6 highlighting the cooperation between these two proteins in maintaining balanced cellular
7 signaling³⁻⁵. In further support of this, the activation of PP2A has been shown to inhibit RAS-
8 driven tumor growth in multiple cell types^{6,7}. PP2A dysregulation in human cancer occurs through
9 multiple mechanisms, including increased expression of endogenous PP2A inhibitor proteins and
10 somatic mutation⁸. The canonical PP2A holoenzyme is comprised of a scaffolding subunit (PP2A
11 A α / β), which serves as the platform for binding of both the catalytic subunit (PP2A C α / β) and
12 one regulatory B subunit, from a distinct set of family members of B's (e.g. B55, B56, B72), which
13 direct PP2A substrate specificity^{9,10}. The PP2A A subunit exists as two isoforms, α and β , and
14 while they share 86% sequence homology they have been suggested to act as functionally distinct
15 proteins^{4,11}. The scaffolding subunit A α is a flexible protein comprised of 15 tandem HEAT
16 (Huntington, Elongation factor 3, A-subunit, TOR) repeats¹². Of these repeats, HEAT 2-8 contact
17 with the regulatory subunits and HEAT 11-15 with the PP2A C subunit.

18 Heterozygous mutations to the PP2A A α subunit are the most common mutations among
19 all PP2A subunits, occur in multiple cancer subtypes, and have been shown to alter holoenzyme
20 formation and regulatory B subunit binding¹³⁻¹⁶. The A α E64D and R418W mutations were shown
21 to result in functional haploinsufficiency through activation of the PI3K/AKT pathway¹⁷. In two
22 independent mouse models, E64D knock-in mice had increased incidence of benzopyrene-induced
23 lung cancer or decreased survival when crossed to KRAS^{G13D} mice^{18,19}. Additionally,

1 characterization of recurrent A α mutations in endometrial cancer has shown that the S256F
2 mutation functions in a dominant negative manner through association with the PP2A inhibitor
3 TIPRL and the W257G mutation increased cell migration^{16,20}.

4 Previous reports have focused on understanding the function of recurrent A α mutations in
5 models of endometrial cancer, and while mutational rates to A α are highest in this context,
6 mutations occur across all cancer types. To explore the mechanism by which recurrent A α
7 mutations contribute to cancer progression, we focused our studies on the most common mutation,
8 R183W, which occurs in multiple cellular contexts. Previous studies have only studied this
9 mutation in endometrial cancer and have analyzed the binding of a few specific regulatory
10 subunits^{16,20}. Importantly, the effects of the R183W mutation on the global A α interactome,
11 oncogenic signaling, and *in vivo* tumor growth have not previously been reported.

12 Here we show that expression of this mutation in a mammary model of transformation and
13 a colon cancer cell line resulted in loss of PP2A tumor suppressive activity, indicating enhanced
14 oncogenic signaling. Biophysical studies demonstrated that R183W caused significant structural
15 changes in the A α protein resulting in altered PP2A activity through reduced catalytic activity, the
16 loss of interaction with tumor suppressive PP2A B regulatory subunits, and the gain of association
17 with Striatin subunits. Global phosphoproteomic profiling of R183W expressing cells revealed
18 activation of the MAPK pathway, subsequently confirmed by western blotting. Accompanying
19 these changes, R183W expressing cells were less sensitive to MEK inhibitors. Combined, our data
20 suggests a mechanism by which the most common PP2A mutation in human cancer potentiates
21 RAS signaling and decreases sensitivity to MEK inhibitors.

22

23

1 **Methods**

2 *Cell Lines and Treatment.* Human cancer cell lines, SW620, H358, and H293T, were purchased
3 from ATCC, UT89 was generated from a primary recurrent uterine serous tumor in the laboratory
4 of Dr. Analisa DiFeo. SW620 and H358 were cultured in RPMI, H293T and UT89 were cultured
5 in DMEM. All media was supplemented with 10% FBS (ThermoFisher, SH3007003) and 1%
6 penicillin/streptomycin (GE Healthcare, SV30010). HMECs were obtained from Dr. Mark
7 Jackson. Specimen 48R and derivatives were grown as described previously^{21,22}. HMEC
8 derivatives were generated as previously described^{21,23}. All cells were grown in a humidified
9 atmosphere containing 5% CO₂. All cells lines underwent monthly testing for mycoplasma
10 contamination (Lonza, LT07-710). AZD-6244 (Selleck Chemical, S1008) was dissolved in DMSO
11 to a concentration of 80 mM and stored at -20°C (for *in vitro* studies).

12 *Clonogenic Assays.* 500 HMEC M/R cells were plated in 6-well plates and grown for 10 days. For
13 treatment studies, cells were treated with vehicle (DMSO) or AZD-6244 for 10 days. Colonies
14 were fixed in a solution of 10% acetic acid and 10% methanol, stained with crystal violet (1%
15 crystal violet in methanol), and counted using ImageJ.

16 *Constructs and Mutagenesis.* Gateway V5-tagged lentiviral expression vector pLX304-PP2A-A α
17 was obtained by DNASU Plasmid Repository (HsCD00444402) deposited by The ORFeome
18 Collaboration²⁴. pLX304-PP2A-A α was sequence verified to be wild type. pLX304-EGFP was
19 created by Gateway cloning EGFP into pLX304 vector. pLX304-PP2A-A α -R183W was generated
20 by site directed mutagenesis (Agilent, 210513). After cloning and mutagenesis all constructs were
21 sequence verified by Sanger sequencing.

1 *Virus Production and Infection.* Lentiviruses were packaged in 293T cells using X-tremeGENE
2 transfection reagent (Sigma, 63666244001) and the second-generation packaging constructs
3 pMD2.G (Addgene, 12259) and psPAX2 (Addgene, 12260). Supernatant media containing virus
4 was collected at 24-48 hours and supplemented with 4 µg/mL polybrene (Santa Cruz, sc-134220).
5 Cells were transduced for 24 hours and cultured for 48 hours before being selected with 4 µg/mL
6 (HMEC cell lines) or 16 µg/mL of Blasticidin (SW620, H358 and UT89) (Invivogen, ant-bl-5b).

7 *Immunoblot Analysis.* Whole cell extracts were prepared by incubating cell pellets in RIPA lysis
8 buffer (ThermoFisher, P189901). Tumor extracts were prepared by mechanical homogenization
9 of tissue in TPER tissue protein extraction reagent (ThermoFisher, 78510). All lysis buffers were
10 supplemented with protease and phosphatase inhibitors (Roche, 05892791 & 09406837). Protein
11 concentrations of cell extracts was determined by Pierce BCA Protein Assay (ThermoFisher,
12 23250) and equal quantities of protein were separated by SDS/PAGE 12% polyacrylamide gels
13 (Bio-Rad, 456-8045) and transferred to nitrocellulose membranes (Bio-Rad, 1704158). Primary
14 antibodies used in this study can be found in Table S2. Primary antibodies were detected with goat
15 anti-mouse obtained from Abcam (ab131368) or donkey anti-rabbit conjugated to horseradish
16 peroxidase obtained from GE Healthcare (NA934), using the Bio-Rad ChemiDoc XRS
17 chemiluminescence imager. Densitometry quantification was performed within the Bio-Rad Image
18 Lab software.

19 *V5 Affinity Purification-Mass Spectrometry (AP-MS) and Co-Immunoprecipitation Analysis.*
20 SW620, HMEC, H358, and OV89 stable cell lines were plated to 70% confluency in 150 mm
21 plates. After 24 hours, cells were harvested and co-immunoprecipitation was performed per Dyna-
22 beads Co-Immunoprecipitation protocol (ThermoFisher, 14321D). V5 antibody (Abcam,
23 ab27671) was coupled at a concentration of 7 µg/mg of Dyna-beads. Following incubation of the

1 antibody-coupled Dyna-beads with cell lysate, half of the beads were reserved for mass
2 spectrometry analysis and the remaining half was eluted for Immunoblot analysis. Digestion for
3 AP-MS samples were performed using an on-bead digestion protocol. Briefly, magnetic beads
4 were washed 3 times with 100mM Tris-EDTA (pH 8) and supernatant removed. Thirty microliters
5 of 100mM Tris-EDTA (pH 8) was added to beads. Bead-bound proteins were reduced with 10mM
6 dithiothreitol for 1-hour at 37°C, followed by alkylation with 25mM iodoacetamide for 30min in
7 the dark. After reduction/alkylation of proteins a dual digestion was performed with 0.3
8 micrograms of lysyl endopeptidase on a dry bath shaker for 1 hour at 37°C followed by the addition
9 of 0.3 micrograms of trypsin with incubation overnight at 37°C. After digestion, samples were
10 filtered with 0.22µM spin filters to remove any particulates prior to MS analysis (Costar Spin-X,
11 Sigma-Aldrich). Peptides were sequenced using data dependent MS acquisition (DDA) as
12 previously described²⁵. Fresh conjugated beads were prepared for each biological replicate, three
13 biological replicates were performed for each experiment.

14 *AP-MS Interaction Scoring and Data Visualization.* SAINTexpress AP-MS software, accessible
15 through the CRAPome, was used to filter and score interactions using three replicates of EGFP-
16 V5 (per cell line) as a negative control^{26,27}. Default SAINT express options were utilized.
17 SAINTexpress files were uploaded to ProHits-viz for data visualization and dot plot generation²⁸.
18 The default ProHits-viz options were *primary filter* = 0.01 and *secondary filter* = 0.05
19 (corresponding to FDR), with a *minimum abundance value* = 0 and a *maximum abundance value*
20 = 50. No normalization or log transformation was utilized for data visualization.

21 *Phosphatase Activity Assay.* HMEC M/R stable cell lines were plated to 70% confluency in 150
22 mm plates. After 24 hours, cells were lysed in phosphatase buffer consisting of 25 mM HEPES, 1
23 mM MgCl, 0.1 mM MnCl, 1% Triton-X, and protease inhibitor. 5 mg of protein lysate was

1 incubated with 1.5 mg of V5-antibody conjugated beads (described above) and incubated on a
2 roller for 30 min at 4°C. Beads were washed 3X with phosphatase assay buffer consisting of 25
3 mM HEPES, 1 mM MgCl₂, and 0.1 mM MnCl₂. Following washes, an aliquot of the beads was
4 reserved for Western blotting. For the phosphatase assay, the remaining beads were resuspended
5 in phosphatase assay buffer supplemented with 1 mM DTT (100 μL/1 mg) and incubated with
6 increasing concentrations of DiFMUP (ThermoFisher, D6567) on a shaker for 15 min at 37°C.
7 Fluorescence was measured at 365/455 nm. Measurements taken from V5-EGFP expressing cells
8 were used to subtract background. Rate of phosphatase activity was calculated by fluorescent units
9 divided by the incubation time (fluorescent units/min). Final activity was normalized to the total
10 PP2A C subunit levels in the IP material determined by Western blot.

11 *Xenograft Tumor Formation and AZD-6244 Treatment Studies.* 5x10⁶ SW620 cells were injected
12 subcutaneously in 50% matrigel into the right flanks of 6-8-week-old female Balb/c *nu/nu* mice.
13 Tumors were allowed to grow to 100 mm³, then randomized into control or AZD-6244 (25 mg/kg
14 BID) treatment groups and tumor volume was assessed by caliper measurement every other day.
15 Tumor tissue was harvested two hours after the final dose of the treatment study. Tumor tissue
16 was both formalin-fixed, for IHC, and snap frozen in liquid nitrogen for immunoblotting and
17 phosphoproteomics analysis. For *in vivo* treatment studies, AZD-6244 was dissolved in 10%
18 DMA, 10% solutol, and water.

19 *Phosphoproteomics.* Sections from three tumors representative of the average tumor growth of
20 each group from the SW620 xenograft were utilized for phosphoproteomic analysis. Tissue was
21 rinsed with 1xPBS to remove any residual blood contaminated prior to sample preparation. Tissue
22 was subsequently solubilized with 2% Sodium dodecyl sulfate (SDS) containing protease and
23 phosphatase inhibitors. Detergent removal was performed using the FASP cleaning procedure and

1 eight hundred micrograms of each sample was digested enzymatically with a two-step
2 LysC/trypsin digestion²⁹. Phosphopeptides were enriched with titanium dioxide and analyzed by
3 LC-MS/MS using a UPLC system (NanoAcquity, Waters) that was interfaced to Orbitrap
4 ProVelos Elite mass spectrometer (Thermo Fisher) and quantified as previously described³⁰.

5 *KSEA and Pathway Analysis.* KSEA analysis was based on the approach originally described by
6 Casado *et al.* and executed with the “KSEAapp” R package version 0.99.0, available through the
7 CRAN repository, with the `NetworKIN = FALSE` feature applied^{31,32}. Pathway analysis was
8 performed at the protein level using the Reactome database of pathways³³. Each protein was
9 represented by the phosphopeptide with the most significant one-way ANOVA p-value across all
10 the groups. One-sided Fisher’s exact test was used to calculate the pathway enrichment of proteins
11 that have a $\log_2(\text{fold change})$ of (A) 1.5 or greater for enrichment of hyper-phosphorylated*
12 proteins or (B) -1.5 or lower for enrichment of dephosphorylated* proteins. Fold change was
13 calculated relative to EGFP. All calculations and related plots were performed/generated in R
14 version 3.3.2. *Due to the absence of a total protein arm in the phosphoproteomics experiment, we
15 cannot confirm if each protein’s abundance is altered amongst the different conditions; thus, the
16 “hyper-phosphorylated” and “dephosphorylated” terms are used with the assumption that there is
17 no underlying change in the total protein level between the two compared conditions.

18 *Molecular Dynamics Simulations.* Structural coordinates of PP2A were downloaded from the
19 PDB. (ID 2IAE). The R183W mutant was constructed *in silico* using the ICM mutagenesis
20 software³⁴. The systems were prepared for simulations using the High-throughput Molecular
21 Dynamics (HTMD) package³⁵. The systems were defined using Amber99SB14 force field,
22 employing explicit TIP3P water molecules as solvent^{36,37}. The systems were minimized with 1000
23 steps of steepest descent integrator and equilibrated in the NPT ensemble for 5 ns, using a

1 Berendsen barostat at 1 atm³⁸. The temperature was kept at 300 K° by a Langevin thermostat. A
2 1050 ns production run was carried out for all the systems in the NVT ensemble with a time step
3 of 4 fs. All the simulations were carried out with the ACEMD program³⁹. Well-Tempered
4 Metadynamics (WTMetaD) of the A subunit wild-type and mutant structure was performed at 300
5 K using the software ACEMD and the PLUMED plugin using an integration step of 4 fs⁴⁰. To
6 study the influence of R183 and R183W mutant on the conformation of the A subunit, we chose
7 the dihedral angles of the WT/mutated residue to be the collective variable (CV). The choice of
8 the CVs (CV1 = phi and CV2 = psi) was based on the observation that the slowest motions in a
9 protein are a function of their backbone flexibility⁴¹. Therefore, the differences in the structural
10 effects resulting from the changes between wild-type and the mutant should be pronounced in the
11 dihedral angles. A total of 450 ns in the NVT ensemble were needed to reach full convergence of
12 the free energy. The free energy surface of the WTMetaD simulation as a function of the two CVs
13 is readily obtained by integrating the deposited energy bias along the trajectory. The error on the
14 minima and barriers of the free energy surface was estimated from the largest variation observed
15 in the mono-dimensional projections along the collective variables during the last 100 ns of the
16 simulation. It amounts to 0.5 kcal/mol.

17 The structures corresponding to the minima were selected from the WTMetaD trajectories,
18 based on the values of collective variables CV1 and CV2 using analysis tool of the GROMACS
19 package⁴². The structural figures were generated using VMD, ICM-Pro and PyMol softwares^{34,43,44}.

20
21
22
23
24

1 **Results**

2 *R183 is the most commonly mutated residue of PP2A A α*

3 In human tumors, 374 heterozygous missense mutations have been identified in the PP2A
4 A α subunit (as of June 2018 from cBioPortal.org). The overall somatic mutation frequency to A α
5 across all cancers is approximately 1%, and interestingly, the distribution of mutations in the PP2A
6 scaffold subunit is nonrandom, resulting in a mutational hotspot within HEAT 5 of the protein
7 **(Figure 1A)**^{13,14,45-47}. The most commonly mutated residue to the A α scaffolding protein is Arg-
8 183, and mutation to this residue results in either a tryptophan (R183W) or a glutamine (R183Q)
9 at this position, with tryptophan (R183W) occurring most frequently **(Figure 1A)**. Mutation to a
10 glycine (R183G), has been reported in smaller sequencing cohorts, but has not been identified in
11 larger whole genome sequencing efforts^{14,48}. Arg-183 mutations are recurrent in multiple cancer
12 types, with the majority of these found in colorectal (CRC), uterine, and breast cancers **(Figure**
13 **1B)**.

14 *A α R183W alters the PP2A interactome and protein conformation*

15 PP2A inactivation has been shown to fully transform human epithelial cells expressing
16 RAS⁵. Additionally, analysis of sequencing data available on cBioPortal revealed that the R183W
17 mutation coexists with KRAS mutations at a significant frequency in patient tumors
18 **(Supplemental Figure 1)**. To evaluate the relevance of the PP2A A α R183W mutation in RAS
19 driven models, we used the KRAS mutant colorectal cancer cell line SW620 as well as a RAS
20 dependent human mammary epithelial cell (HMEC) model of transformation, shp16-shp53-
21 Myc/RAS cells (M/R), described previously²¹. We stably expressed V5-tagged WT or R183W A α
22 into the transformed shp16-shp53-Myc/RAS cells (M/R) and SW620 cells using a lentiviral
23 approach. Given that studies have shown that PP2A A α mutations result in altered holoenzyme

1 complex formation and A α interactome^{16,19,20}, we first used co-immunoprecipitation of V5-tagged
2 WT or R183W A α protein in our cell models, SW620 and M/R cells, followed by mass
3 spectrometry analysis (AP-MS) to determine the effect of the R183W A α mutation on global
4 protein interactions, and confirmed select changes by immunoblotting (**Figure 2, A-E and**
5 **Supplemental Figure 2, A and B**). Consistent with published literature, the R183W mutation lost
6 the majority of B56 (B'), B55 (B) and B'' family member binding, while also resulting in an
7 increased binding to Striatin family members (B''') (**Figure 2 A-E, Supplemental Figure 2C**).
8 Beyond impacting the binding of PP2A subunits, mass spectrometry analysis identified differential
9 binding of additional proteins, including STRIPAK components and members of the Integrator
10 Complex (**Figure 2A**). Additionally, the R183W mutation did not have a significant impact on C
11 subunit binding when the co-immunoprecipitation was quantified by mass spectrometry (**Figure**
12 **2A**) or by immunoblot following co-immunoprecipitation (**Figure 2C and D**). These changes to
13 the A α interactome were consistent in two additional cell lines, H358 (non-small cell lung cancer)
14 and UT89 (primary uterine serous cancer) (**Supplemental Figure 3, A-C**). We performed a
15 binding assay in a cell free system with recombinant A/C dimer and B56 α . Incubation of
16 recombinant wild type or mutant R183W A/C with B56 α tagged beads confirmed the R183W
17 mutant A/C dimer fails to bind B56 α *in vitro* (**Supplemental Figure 2C**). To determine the effects
18 of the R183W mutation on PP2A activity, we performed phosphatase activity assays using
19 DiFMUP on co-immunoprecipitated lysates from WT and mutant R183W A α expressing M/R cell
20 lines (**Figure 2F and Supplemental Figure 4, A-D**). We calculated Michaelis-Menten kinetics
21 for the WT and mutant R183W A α protein, revealing that while K_m was relatively unchanged with
22 the R183W mutation, V_{max} was substantially decreased. This indicated that while the R183W A α
23 mutation did not affect the affinity of DiFMUP for PP2A, the maximal rate of catalysis was

1 reduced (**Figure 2F and Supplemental Figure 4E**). The striking differences in the interactome
2 and the activity of the WT and R183W A α proteins led us to investigate the possible structural
3 explanations for these differences. We performed molecular dynamics simulations of WT and
4 R183W A α to identify stable protein conformations. The free energy landscape plots were
5 generated as a function of ϕ and ψ dihedral angles of the residues R183 and the mutant R183W
6 (**Figure 2, G and H, Supplemental Figures 5-7**). These landscapes provide evidence that the
7 R183W mutant is capable of exploring an altered free energy landscape to adopt multiple
8 metastable conformations of the A α subunit, which may alter interactions with other proteins.
9 Using these landscapes, we extracted conformations from the most stable conformation of the WT
10 and R183W mutant protein, designated with an “A/B” (**Figure 2, G and H**). These conformations
11 indicate that R183 makes multiple interactions with N211 in the wild type A α protein, which is
12 facilitated by an ion pair interaction between R182 and D215. These interactions are all lost when
13 mutated to a tryptophan. Together, these data show that the R183W mutation to the A α scaffold
14 protein disrupts protein conformation and in turn alters the interactome of this protein.

15 *Introduction of the A α R183W mutation loses growth suppressive phenotype in M/R cells and*
16 *SW620 tumors*

17 Interference of PP2A functions, through altered expression of select subunits or through
18 the expression of SV40 ST antigen, results in cellular transformation^{3,5,49}. To assess the functional
19 role of the recurrent R183W A α mutation on cell growth, we stably expressed V5-tagged WT or
20 R183W A α into the transformed shp16-shp53-Myc/RAS cells (M/R) or SW620 cells using a
21 lentiviral approach (**Figure 3A and 3B**). Clonogenic assays in the M/R cells showed that
22 expression of WT A α significantly decreased the ability of these cells to form 2D colonies, while
23 R183W A α did not maintain these growth suppressive effects (**Figure 3C**). To test the oncogenic

1 potential of R183W A α mutant expressing SW620 cells, we injected these stable isogenic cell
2 lines into a subcutaneous xenograft model of tumorigenesis. While WT A α overexpression
3 resulted in reduced tumor growth *in vivo*, the expression of R183W A α mutant did not mimic this
4 growth suppressive effect (**Figure 3D**). In both models, expression of R183W in cells or tumors
5 caused no growth changes and behaved similarly to the EGFP controls (**Figure 3C and D**). Taken
6 together, our cellular and *in vivo* models suggest that additional expression of WT A α increases
7 PP2A's tumor suppressive function and results in a growth suppressive phenotype which is lost
8 when the R183W mutation is introduced, indicating that the R183W mutation may be loss of
9 function in this context.

10 *Expression of R183W potentiates MAPK signaling in KRAS mutant cells*

11 To determine the impact of the R183W A α mutant on oncogenic signaling, we performed
12 global serine/threonine phosphoproteomics on three tumors which were representative of the
13 average tumor growth for each independent group from the SW620 xenograft study (**Figure 3D**).
14 Overall, we identified and quantified 3860 peptides mapping to 3206 phosphoproteins. To analyze
15 the phosphoproteomic data set, we utilized Kinase Substrate Enrichment Analysis (KSEA)^{31,32}.
16 KSEA uses known kinase-substrate relationships and calculates the potential kinase activity based
17 on the phosphorylation levels of its known substrates. In our data set, this analysis showed an
18 alteration in signaling output of multiple kinases (**Figure 4A and Supplemental Figure 8**). The
19 most significantly altered kinase identified was MAP2K1, or MEK, the kinase responsible for
20 phosphorylating ERK1/2 at T202/Y204. Additionally, MAP2K1 was one of only two kinases
21 shown to be altered when the phosphorylation levels in R183W A α tumors were compared to both
22 WT A α and EGFP (**Figure 4A**). This finding was subsequently confirmed by western blot, where
23 expression of R183W A α resulted in a significant increase in p-ERK levels when compared to

1 either WT A α or control vector expressing tumors (**Figure 4B-D**). In support of this finding,
2 pathway analysis of significantly hyper phosphorylated peptides from the phosphoproteomics
3 results showed enrichment for MAPK/ERK related pathways in the R183W expressing tumors
4 compared to control vector (**Supplemental Figure 9**). To determine the effects of the R183W
5 mutant on oncogenic RAS signaling in the HMEC model of transformation, we performed
6 phospho-specific immunoblotting on p-ERK (T202/Y204) in the isogenic M/R cells. We found
7 significantly increased phosphorylation of p-ERK (T202/Y204) in cells expressing the R183W
8 mutant A α compared to WT cells (**Figure 4E and F**). Interestingly, mutation to the R183 residue
9 most often occurs in colorectal cancer, in which 20-30% of patients have KRAS mutations, and in
10 the identified CRC harboring R183 mutations, 57% had KRAS mutations (**Supplemental Table**
11 **1**), indicating that R183 mutations may co-occur with KRAS mutations in CRC. Taken together,
12 this data confirms the hyper-phosphorylation of ERK upon expression of the R183W *in vitro* and
13 *in vivo* and suggests that inactivation of PP2A by the mutant R183W A α cooperates with the
14 oncogene RAS to potentiate MAPK signaling.

15 *Expression of A α R183W decreases sensitivity to MEK inhibitors*

16 Our results in M/R and SW620 cells indicated that expression of R183W increased MAPK
17 signaling. Additionally, it has been shown recently that inactivation of PP2A through siRNA-
18 mediated silencing of the A subunit results in MEK inhibitor resistance⁷. To determine if the
19 increase in MAPK signaling impacted response to therapy, we treated M/R cells with a MEK
20 inhibitor, AZD-6244, in a colony formation assay. M/R cells expressing A α R183W were less
21 sensitive to MEK inhibition than the parental M/R cells or cells expressing WT A α (**Figure 5A-**
22 **C**). Interestingly, the expression of WT A α increased the sensitivity to MEK inhibition, suggesting
23 that increased PP2A phosphatase activity may enhance the efficacy of kinase inhibitors (**Figure 5**

1 **A-C)**. To determine if these effects were consistent with an *in vivo* model, we treated SW620
2 tumors with AZD-6244 (**Figure 5D**). Although all tumors responded to AZD-6244, after 22 days
3 of treatment, tumors expressing R183W had a significantly larger tumor volume than vector
4 control tumors, while tumors expressing WT were not significantly different than vector control
5 tumors (**Figure 5D and Supplemental Figure 10**). In the SW620 xenograft model, over
6 expression of WT A α did not sensitize tumors to AZD-6244, as was seen in the M/R-WT cell lines
7 by 2D colony formation.

8 Intrinsic resistance to MEK inhibitors has been in part attributed to MEK-ERK reactivation
9 and the activation of parallel oncogenic pathways. AZD-6244 treatment decreased phosphorylated
10 ERK induced by A α R183W, both in the SW620 xenograft and in M/R cells (**Supplemental**
11 **Figure 10 and 11**). Treatment with AZD-6244 resulted in increases in phosphorylation of MEK
12 in both WT and R183W A α expressing cells and tumors, indicating that MEK-ERK reactivation
13 was not a resistance mechanism in this model (**Supplemental Figure 10 and 11**). Compensatory
14 activation of PI3K/AKT/mTOR signaling has been implicated in MEK inhibitor resistance and the
15 dual inhibition of AKT or mTOR and MEK has been shown to enhance apoptosis and tumor
16 growth suppression^{50,51}. Given the baseline alterations in AKT signaling detected in the
17 phosphoproteomics KSEA analysis (**Figure 4B**), we measured phosphorylation levels of the AKT
18 pathway in AZD-6244 treated M/R cells expressing WT or R183W A α . Interestingly, the baseline
19 levels of phosphorylated AKT (S473) were significantly lower in the M/R cells expressing R183W
20 A α (**Supplemental Figure 11**). Upon inhibition of MEK by AZD-6244, the phosphorylation
21 levels of AKT returned to the baseline levels seen in the control or M/R cells expressing WT A α .
22 Taken together, our data suggest that expression of R183W A α decreased the sensitivity of cells
23 and tumors to the MEK inhibitor AZD-6244 and the identified MEK inhibitor resistance

1 mechanism was not mediated through the upregulation of MEK-ERK pathway or robust
2 upregulation of the parallel AKT signaling pathway, suggesting that other PP2A-dependent
3 pathways could be involved in MEK inhibitor resistance.

4 5 **Discussion**

6 The goal of this study was to elucidate the functional role and potential clinical relevance
7 of the PP2A A α R183W mutant in tumorigenesis and response to therapy. Here, we demonstrate
8 that this recurrent PP2A mutation may enhance tumorigenesis through the loss of key tumor
9 suppressive regulatory subunits resulting in potentiation of RAS signaling and decreased
10 sensitivity to MEK inhibitors.

11 Our co-immunoprecipitation assays in several different cellular contexts revealed
12 interaction changes to A α which were conserved across all cell types studied. Despite significantly
13 reduced PP2A catalytic activity, significant changes in PP2A C binding to the R183W mutant were
14 not seen in any cellular context. The R183W mutation also dramatically reduced binding to the
15 majority of the B55, B56 and PR72/PR130 subunit family members. Through molecular modeling
16 we showed a marked conformational change in the R183W mutant A α protein, suggesting that the
17 altered PP2A catalysis and loss of regulatory subunit binding could be, in part, through altered
18 protein conformation. This may be explained by work showing the dynamic and elastic nature of
19 the A subunit can influence catalysis by altering the distance of the B/C interface as well as the
20 orientation of the catalytic residues within the C subunit^{52,53}. Further, it has been proposed that
21 partial unfolding of the A subunit may enhance subunit binding, utilizing a “fly-casting
22 mechanism”⁵³. Future analysis of the R183W mutant protein and how it may impact the dynamic
23 nature of protein folding may help explain the disruption in regulatory subunit and other protein
24 binding partners. Additionally, some of the interaction changes caused by the R183W mutation

1 were context-dependent. For example, a gain in binding of the components of the integrator
2 complex was only detected in the CRC cell line SW620. These context-dependent changes could
3 be associated with the expression of certain proteins within a particular histological subtype and
4 further exploration would be useful in understanding the histological distribution of the R183W
5 mutation at varying frequencies across different cancer types.

6 The study of the effects of PP2A A α subunit mutations on signaling has been limited to
7 analysis of known direct PP2A targets, and the analysis of phosphorylation changes at a global
8 level has remained unexplored. Here, we utilized global phosphoproteomics and subsequent
9 bioinformatics analysis to provide a more comprehensive picture of the pathways and proteins
10 altered upon mutation of *PPP2RIA*. Given the broad biological role of PP2A holoenzymes in
11 cellular signaling cascades, it is unsurprising that a mutation to the common scaffolding subunit
12 would have such broad effects in the phosphoproteome. Additionally, these results suggest the
13 potential role of oncogenic drivers and histological context to affect signaling as the increased
14 ERK phosphorylation and decreased AKT phosphorylation identified in the colorectal SW620 and
15 mammary M/R cells expressing R183W are different than those seen with A α mutations in
16 endometrial cancers¹⁶.

17 Targeting of the ERK-RAS pathway through inhibition of MEK1/2 has been shown to be
18 a promising therapeutic approach in certain cancer subtypes; however, resistance and feedback
19 mechanisms have limited the overall clinical benefit. These resistance mechanisms include parallel
20 pathway activation in response to MEK inhibition, reactivation of the MEK-ERK pathway, and
21 adaptive kinome reprogramming⁵⁴. Our findings show that the R183W A α mutation works in part
22 by potentiating oncogenic RAS signaling, which results in the upregulation of ERK pathway
23 signaling and a decreased sensitivity to MEK inhibitors. However, the identified MEK inhibitor

1 resistance mechanism was not mediated through the upregulation of MEK-ERK pathway or robust
2 upregulation of the parallel AKT signaling pathway, suggesting that other PP2A-dependent
3 pathways could be involved in MEK inhibitor resistance. Tumors expressing mutant R183W A α
4 displayed a global altered phosphoproteome, indicating that the R183W mutant may result in
5 signal re-wiring via multiple mechanisms, including loss or gain of regulatory subunit binding and
6 altered PP2A activity, read out as decreased MEK inhibitor sensitivity. The specifics of this re-
7 wiring and their impact on targeted cancer therapeutics are an area of further investigation.

8 In summary, we show cellular, *in vivo*, and structural evidence that the recurrent PP2A A α
9 mutation, R183W, may enhance tumorigenesis through the loss of key tumor suppressive
10 regulatory subunits and altered PP2A catalytic activity, thereby potentiating oncogenic RAS
11 signaling. In addition, we show that although this recurrent mutation potentiates RAS signaling,
12 these cells were less responsive to MEK inhibition, supporting that mutation to A α , in particular
13 R183W, could be predictive of MEK inhibitor response.

14
15
16
17
18
19
20
21
22
23

1 **Study Approval**

2 All animal experiments were approved by the Institutional Animal Care and Use Committee
3 (IACUC) at Case Western Reserve University. Animal use and care was in strict compliance with
4 institutional guidelines and all experiments conformed to the relevant regulatory standards
5 established by Case Western Reserve University.

6 **Author Contributions**

7 CMO and GN designed the research studies. CMO wrote the manuscript and GN edited the
8 manuscript. CMO, DL, DW, RA, ZW, DS, BB, ET, AU, ST, and SH performed experiments and
9 interpreted the data. JS, A-CG, JW, WX, AD, DB, SH, MJ, and GN provided observations and
10 scientific interpretations. All authors discussed results and provided input on the manuscript.

11 **Acknowledgements**

12 The authors wish to acknowledge the Young Scientist Foundation and the students who worked
13 on this project through this program, including Aditya Upadhyay. This work was partially
14 supported by the NIH/NCI R01CA181654 (to GN) and T32GM00883 (to CMO). This publication
15 was made possible in part by the Clinical and Translational Science Collaborative of Cleveland,
16 4UL1TR000439 from the National Center for Advancing Translational Sciences (NCATS)
17 component of the National Institutes of Health and NIH roadmap for Medical Research. This
18 research was supported by the Athymic Animal and Preclinical Therapeutics and Cytometry &
19 Imaging Microscopy cores of the Case Comprehensive Cancer Center at Case Western Reserve
20 University (funded by NIH P30 CA043703). G. Narla is supported by the Pardee-Gerstacker
21 Professorship in Cancer Research.

22

23

References:

- 1 Kauko, O. *et al.* Label-free quantitative phosphoproteomics with novel pairwise abundance normalization reveals synergistic RAS and CIP2A signaling. *Scientific reports* **5**, 13099, doi:10.1038/srep13099 (2015).
- 2 Rangarajan, A., Hong, S. J., Gifford, A. & Weinberg, R. A. Species- and cell type-specific requirements for cellular transformation. *Cancer cell* **6**, 171-183, doi:10.1016/j.ccr.2004.07.009 (2004).
- 3 Sablina, A. A., Hector, M., Colpaert, N. & Hahn, W. C. Identification of PP2A complexes and pathways involved in cell transformation. *Cancer research* **70**, 10474-10484, doi:10.1158/0008-5472.can-10-2855 (2010).
- 4 Sablina, A. A. *et al.* The tumor suppressor PP2A A β regulates the RalA GTPase. *Cell* **129**, 969-982, doi:10.1016/j.cell.2007.03.047 (2007).
- 5 Chen, W. *et al.* Identification of specific PP2A complexes involved in human cell transformation. *Cancer cell* **5**, 127-136 (2004).
- 6 Sangodkar, J. *et al.* Activation of tumor suppressor protein PP2A inhibits KRAS-driven tumor growth. *The Journal of clinical investigation* **127**, 2081-2090, doi:10.1172/jci89548 (2017).
- 7 Kauko, O. *et al.* PP2A inhibition is a druggable MEK inhibitor resistance mechanism in KRAS-mutant lung cancer cells. *Science translational medicine* **10**, doi:10.1126/scitranslmed.aag1093 (2018).
- 8 Seshacharyulu, P., Pandey, P., Datta, K. & Batra, S. K. Phosphatase: PP2A structural importance, regulation and its aberrant expression in cancer. *Cancer letters* **335**, 9-18, doi:10.1016/j.canlet.2013.02.036 (2013).
- 9 Shi, Y. Serine/threonine phosphatases: mechanism through structure. *Cell* **139**, 468-484, doi:10.1016/j.cell.2009.10.006 (2009).
- 10 Sangodkar, J. *et al.* All roads lead to PP2A: exploiting the therapeutic potential of this phosphatase. *The FEBS journal* **283**, 1004-1024, doi:10.1111/febs.13573 (2016).
- 11 Zhou, J., Pham, H. T., Ruediger, R. & Walter, G. Characterization of the A α and A β subunit isoforms of protein phosphatase 2A: differences in expression, subunit interaction, and evolution. *The Biochemical journal* **369**, 387-398, doi:10.1042/bj20021244 (2003).
- 12 Groves, M. R., Hanlon, N., Turowski, P., Hemmings, B. A. & Barford, D. The structure of the protein phosphatase 2A PR65/A subunit reveals the conformation of its 15 tandemly repeated HEAT motifs. *Cell* **96**, 99-110 (1999).
- 13 Calin, G. A. *et al.* Low frequency of alterations of the alpha (PPP2R1A) and beta (PPP2R1B) isoforms of the subunit A of the serine-threonine phosphatase 2A in human neoplasms. *Oncogene* **19**, 1191-1195, doi:10.1038/sj.onc.1203389 (2000).
- 14 Shih Ie, M. *et al.* Somatic mutations of PPP2R1A in ovarian and uterine carcinomas. *The American journal of pathology* **178**, 1442-1447, doi:10.1016/j.ajpath.2011.01.009 (2011).
- 15 Ruediger, R., Pham, H. T. & Walter, G. Alterations in protein phosphatase 2A subunit interaction in human carcinomas of the lung and colon with mutations in the A β subunit gene. *Oncogene* **20**, 1892-1899, doi:10.1038/sj.onc.1204279 (2001).
- 16 Haesen, D. *et al.* Recurrent PPP2R1A Mutations in Uterine Cancer Act through a Dominant-Negative Mechanism to Promote Malignant Cell Growth. *Cancer research* **76**, 5719-5731, doi:10.1158/0008-5472.can-15-3342 (2016).

- 1 17 Chen, W., Arroyo, J. D., Timmons, J. C., Possemato, R. & Hahn, W. C. Cancer-
2 associated PP2A Aalpha subunits induce functional haploinsufficiency and
3 tumorigenicity. *Cancer research* **65**, 8183-8192, doi:10.1158/0008-5472.Can-05-1103
4 (2005).
- 5 18 Walter, G. & Ruediger, R. Mouse model for probing tumor suppressor activity of protein
6 phosphatase 2A in diverse signaling pathways. *Cell cycle (Georgetown, Tex.)* **11**, 451-
7 459, doi:10.4161/cc.11.3.19057 (2012).
- 8 19 Ruediger, R., Ruiz, J. & Walter, G. Human cancer-associated mutations in the Aalpha
9 subunit of protein phosphatase 2A increase lung cancer incidence in Aalpha knock-in and
10 knockout mice. *Molecular and cellular biology* **31**, 3832-3844, doi:10.1128/mcb.05744-
11 11 (2011).
- 12 20 Jeong, A. L. *et al.* Patient derived mutation W257G of PPP2R1A enhances cancer cell
13 migration through SRC-JNK-c-Jun pathway. *Scientific reports* **6**, 27391,
14 doi:10.1038/srep27391 (2016).
- 15 21 Junk, D. J., Cipriano, R., Bryson, B. L., Gilmore, H. L. & Jackson, M. W. Tumor
16 microenvironmental signaling elicits epithelial-mesenchymal plasticity through
17 cooperation with transforming genetic events. *Neoplasia (New York, N.Y.)* **15**, 1100-1109
18 (2013).
- 19 22 Garbe, J. C. *et al.* Molecular distinctions between stasis and telomere attrition senescence
20 barriers shown by long-term culture of normal human mammary epithelial cells. *Cancer*
21 *research* **69**, 7557-7568, doi:10.1158/0008-5472.can-09-0270 (2009).
- 22 23 Cipriano, R. *et al.* TGF-beta signaling engages an ATM-CHK2-p53-independent RAS-
23 induced senescence and prevents malignant transformation in human mammary epithelial
24 cells. *Proc Natl Acad Sci U S A* **108**, 8668-8673, doi:10.1073/pnas.1015022108 (2011).
- 25 24 Wiemann S, P. C., Hu Y, Hunter P, Harbers M, Amiet A, Bethel G, Busse M, Carninci P,
26 Dunham I, Hao T, Harper JW, Hayashizaki Y, Heil O, Hennig S, Hotz-Wagenblatt A,
27 Jang W, Jöcker A, Kawai J, Koenig C, Korn B, Lambert C, LeBeau A, Lu S, Maurer J,
28 Moore T, Ohara O, Park J, Rolfs A, Salehi-Ashtiani K, Seiler C, Simmons B, van
29 Brabant Smith A, Steel J, Wagner L, Weaver T, Wellenreuther R, Yang S, Vidal M,
30 Gerhard DS, LaBaer J, Temple G, Hill DE. The ORFeome Collaboration: a genome-scale
31 human ORF-clone resource. *Nature methods* **13**, 191-192, doi:10.1038/nmeth.3776
32 (2016).
- 33 25 Schlatzer, D. *et al.* A Targeted Mass Spectrometry Assay for Detection of HIV Gag
34 Protein Following Induction of Latent Viral Reservoirs. *Analytical chemistry* **89**, 5325-
35 5332, doi:10.1021/acs.analchem.6b05070 (2017).
- 36 26 Mellacheruvu, D. *et al.* The CRAPome: a contaminant repository for affinity purification-
37 mass spectrometry data. *Nature methods* **10**, 730-736, doi:10.1038/nmeth.2557 (2013).
- 38 27 Morris, J. H. *et al.* Affinity purification-mass spectrometry and network analysis to
39 understand protein-protein interactions. *Nature protocols* **9**, 2539-2554,
40 doi:10.1038/nprot.2014.164 (2014).
- 41 28 Knight, J. D. R. *et al.* ProHits-viz: a suite of web tools for visualizing interaction
42 proteomics data. *Nature methods* **14**, 645-646, doi:10.1038/nmeth.4330 (2017).
- 43 29 Wisniewski, J. R., Zougman, A., Nagaraj, N. & Mann, M. Universal sample preparation
44 method for proteome analysis. *Nature methods* **6**, 359-362, doi:10.1038/nmeth.1322
45 (2009).

1 30 McClinch, K. *et al.* Small-Molecule Activators of Protein Phosphatase 2A for the
2 Treatment of Castration-Resistant Prostate Cancer. *Cancer research* **78**, 2065-2080,
3 doi:10.1158/0008-5472.can-17-0123 (2018).

4 31 Casado, P. *et al.* Kinase-substrate enrichment analysis provides insights into the
5 heterogeneity of signaling pathway activation in leukemia cells. *Science signaling* **6**, rs6,
6 doi:10.1126/scisignal.2003573 (2013).

7 32 Wiredja, D. D., Koyuturk, M. & Chance, M. R. The KSEA App: a web-based tool for
8 kinase activity inference from quantitative phosphoproteomics. *Bioinformatics (Oxford,*
9 *England)*, doi:10.1093/bioinformatics/btx415 (2017).

10 33 Fabregat, A. *et al.* The Reactome pathway Knowledgebase. *Nucleic acids research* **44**,
11 D481-487, doi:10.1093/nar/gkv1351 (2016).

12 34 Abagyan, R., Totrov, M. & Kuznetsov, D. ICM- A new method for protein modeling and
13 design: Applicataions to docking and structure prediction from the distorted native
14 conformation. *Journal of computational chemistry* **15**, 488-506 (1994).

15 35 Doerr, S., Harvey, M. J., Noe, F. & De Fabritiis, G. HTMD: High-Throughput Molecular
16 Dynamics for Molecular Discovery. *Journal of chemical theory and computation* **12**,
17 1845-1852, doi:10.1021/acs.jctc.6b00049 (2016).

18 36 Case, D. A. *et al.* The Amber biomolecular simulation programs. *Journal of*
19 *computational chemistry* **26**, 1668-1688, doi:10.1002/jcc.20290 (2005).

20 37 Price, D. J. & Brooks, C. L., 3rd. A modified TIP3P water potential for simulation with
21 Ewald summation. *The Journal of chemical physics* **121**, 10096-10103,
22 doi:10.1063/1.1808117 (2004).

23 38 Berendsen, H. J. C., Postma, J. P. M., Gunsteren, W. F. v., DiNola, A. & Haak, J. R.
24 Molecular dynamics with coupling to an external bath. *The Journal of chemical physics*
25 **81**, doi:1.448118 (1984).

26 39 Harvey, M. J., Giupponi, G. & Fabritiis, G. D. ACEMD: Accelerating Biomolecular
27 Dynamics in the Microsecond Time Scale. *Journal of chemical theory and computation*
28 **5**, 1632-1639, doi:10.1021/ct9000685 (2009).

29 40 Bonomi, M., Barducci, A. & Parrinello, M. Reconstructing the equilibrium Boltzmann
30 distribution from well-tempered metadynamics. *Journal of computational chemistry* **30**,
31 1615-1621, doi:10.1002/jcc.21305 (2009).

32 41 Skliros, A. *et al.* The importance of slow motions for protein functional loops. *Physical*
33 *biology* **9**, 014001, doi:10.1088/1478-3975/9/1/014001 (2012).

34 42 Hess, B., Kutzner, C., van der Spoel, D. & Lindahl, E. GROMACS 4: Algorithms for
35 Highly Efficient, Load-Balanced, and Scalable Molecular Simulation. *Journal of*
36 *chemical theory and computation* **4**, 435-447, doi:10.1021/ct700301q (2008).

37 43 DeLano, W. PyMOL molecular viewer: Updates and refinements. *Abstracts of Papers of*
38 *the American Chemical Society* **238** (2009).

39 44 Humphrey, W., Dalke, A. & Schulten, K. VMD: visual molecular dynamics. *Journal of*
40 *molecular graphics* **14**, 33-38, 27-38 (1996).

41 45 Kamburov, A. *et al.* Comprehensive assessment of cancer missense mutation clustering
42 in protein structures. *Proc Natl Acad Sci U S A* **112**, E5486-5495,
43 doi:10.1073/pnas.1516373112 (2015).

44 46 Rahman, M. *et al.* PPP2R1A mutation is a rare event in ovarian carcinoma across
45 histological subtypes. *Anticancer research* **33**, 113-118 (2013).

1 47 Hoang, L. N. *et al.* Targeted mutation analysis of endometrial clear cell carcinoma.
2 *Histopathology* **66**, 664-674, doi:10.1111/his.12581 (2015).

3 48 Jones, S. *et al.* Frequent mutations of chromatin remodeling gene ARID1A in ovarian
4 clear cell carcinoma. *Science (New York, N.Y.)* **330**, 228-231,
5 doi:10.1126/science.1196333 (2010).

6 49 Pallas, D. C. *et al.* Polyoma small and middle T antigens and SV40 small t antigen form
7 stable complexes with protein phosphatase 2A. *Cell* **60**, 167-176 (1990).

8 50 Holt, S. V. *et al.* Enhanced apoptosis and tumor growth suppression elicited by
9 combination of MEK (selumetinib) and mTOR kinase inhibitors (AZD8055). *Cancer*
10 *research* **72**, 1804-1813, doi:10.1158/0008-5472.can-11-1780 (2012).

11 51 Roberts, P. J. *et al.* Combined PI3K/mTOR and MEK inhibition provides broad
12 antitumor activity in faithful murine cancer models. *Clinical cancer research : an official*
13 *journal of the American Association for Cancer Research* **18**, 5290-5303,
14 doi:10.1158/1078-0432.ccr-12-0563 (2012).

15 52 Grinthal, A., Adamovic, I., Weiner, B., Karplus, M. & Kleckner, N. PR65, the HEAT-
16 repeat scaffold of phosphatase PP2A, is an elastic connector that links force and catalysis.
17 *Proc Natl Acad Sci U S A* **107**, 2467-2472, doi:10.1073/pnas.0914073107 (2010).

18 53 Tsytlonok, M. *et al.* Complex energy landscape of a giant repeat protein. *Structure*
19 *(London, England : 1993)* **21**, 1954-1965, doi:10.1016/j.str.2013.08.028 (2013).

20 54 Caunt, C. J., Sale, M. J., Smith, P. D. & Cook, S. J. MEK1 and MEK2 inhibitors and
21 cancer therapy: the long and winding road. *Nature reviews. Cancer* **15**, 577-592,
22 doi:10.1038/nrc4000 (2015).

23

24

25

26

27

28

29

30

31

32

33

34

35

36

37

38

1 **Figure Legends**

2 **Figure 1. R183W is the most commonly mutated residue of PP2A A α across human cancer. (A)**

3 Representation of all identified heterozygous missense mutations to the A α subunit distributed across the
4 length of the protein. The y-axis shows the number of mutations and the type of mutations are represented
5 by colored dots. Green dots indicate missense mutations, black dots indicate nonsense mutations, and purple
6 dots indicate splice site mutations and truncations (adapted from cBioportal.org). Binding regions relevant
7 to A α are indicated by the colored boxes. Yellow indicates regulatory subunit binding regions, yellow with
8 grey lines indicate the region within the regulatory subunit binding region where SV40 small T antigen
9 binds, and blue indicates the catalytic subunit binding region. **(B)** The distribution of all heterozygous
10 missense mutations to the R183 residue by histological subtype.

11

12 **Figure 2. A α R183W alters the PP2A interactome and decreases PP2A activity. (A)**

13 of V5 tagged wild type or R183W A α protein from SW620 cells. Statistical analysis performed by SAINT
14 and visualization performed using ProHits-viz (n=3). **(B and C)** Co-immunoprecipitation of V5-tagged
15 wild type or R183W A α protein to determine binding of select PP2A family members from SW620 cells
16 **(B)** and M/R cells **(C)**. **(D and E)** Quantification of relative binding of PP2A subunit family members from
17 co-immunoprecipitation of V5-tagged wild type or R183W A α protein in SW620 **(D)** or M/R **(E)** cells.
18 Binding normalized to V5 levels and plotted relative to wild type A α , n=3 (Multiple T-tests, with Holm-
19 Sidak method of correction for multiple comparisons: p-values: * \leq 0.05, ** \leq 0.01, *** \leq 0.001,
20 **** \leq 0.0001). **(F)** PP2A activity assay of WT (purple) and mutant R183W (red) A α holoenzymes. Briefly,
21 V5-tagged WT and R183W A α protein was co-immunoprecipitated and the resulting IPs, including co-
22 immunoprecipitated proteins, were incubated for 15 minutes with increasing concentrations of DiFMUP and
23 analyzed for activity by fluorescence, data presented as the mean \pm SD (n=3). **(G)** Free energy surface
24 (FES) plot of the WT A α subunit, as calculated from Well Tempered-metadynamics simulations. The two
25 minima have been labelled as A and B. The representative structure of the clustered conformations in the

1 minima has been illustrated. In the minimum, the side chain of R183 makes interactions with the side chain
2 of N211. This interaction is facilitated by an ion pair interaction between R182 and D215. **(H)** Free energy
3 surface (FES) plot of the R183W mutant A α subunit, as calculated from Well Tempered-metadynamics
4 simulations. The deepest minimum has been labelled as A. The representative structure of the clustered
5 conformations in the minima has been illustrated. In the minimum, the side chain of R183W mutant makes
6 interactions with the backbone carbonyl oxygen atom of S219. The loss of interactions as a result of the
7 mutation pushes the A subunit into a conformation that is not observed in the WT R183 PP2A A α subunit.

8

9 **Figure 3. The R183W mutation loses growth suppressive activity compared to wild type PP2A. (A)**

10 Western blot validation of A and C subunit expression levels from M/R stable cell lines and quantification,
11 data presented as mean \pm SD (n=3). **(B)** Western blot validation of A and C subunit expression levels from
12 SW620 stable cell lines and quantification, data presented as mean \pm SD (n=3). **(C)** Clonogenic assay of
13 M/R cells, briefly, 500 cells were seeded in 6 well plates and allowed to grow for 10 days, then fixed,
14 stained with crystal violet, and quantified via ImageJ. Three technical replicates per biological replicate,
15 data represented as the mean \pm SD (n=4). (One-way ANOVA; Tukey's correction for multiple comparisons,
16 p-values: * $<$ 0.05, ** \leq 0.01). **(D)** Xenograft assay of SW620 cells expressing EGFP (control vector) (n=10),
17 wild type A α (n=10) or A α -R183W (n=9), injected subcutaneously into the flanks of female nude mice.
18 Tumors were measured every other day. Data are presented as mean \pm SEM (Students T-tests, R183W
19 relative to WT, p-values: * $<$ 0.05, ** \leq 0.01).

20

21 **Figure 4. A α -R183W expression alters the phosphoproteome and increases MAPK signaling. (A)**

22 Three tumors from each group of the SW620 xenograft were analyzed for global serine/threonine
23 phosphoproteomics. Kinase-Substrate Enrichment Analysis (KSEA) was performed on the
24 phosphoproteomic dataset to estimate relative changes in kinase activity. The normalized kinase scores are
25 color coded in the heat map; blue = negative score. meaning a decrease in kinase activity in the experimental

1 group (numerator of the fold change) relative to the reference group (denominator). Inversely, red = positive
2 score, which is an increase in kinase activity in the experimental group (numerator) relative to the reference
3 (denominator). White = zero, no change between the groups (Asterisks mark the scores with p-value < 0.05,
4 as calculated by a z-test. Only kinases with at least 3 identified substrates are illustrated). **(B)** Table showing
5 identified phosphorylated substrates and phosphosites of MAP2K1 from the KSEA analysis. **(C)** Western
6 blot validation and quantification of phosphorylated and total ERK and MEK levels in SW620 tumors. **(D)**
7 Quantification of phospho-ERK relative to total ERK in cohort of SW620 tumors expressing EGFP, A α
8 WT, and A α R183W. Ratio of phospho/total levels is plotted relative to one EGFP tumor, data are presented
9 as mean \pm SD, (One-way ANOVA; Tukey's correction for multiple comparisons, p-values: * < 0.05, ** \leq
10 0.01). **(E)** Representative Western blot of p-ERK and total ERK in HMEC cells. **(F)** Quantification of
11 phospho-ERK relative to total ERK from M/R-WT and M/R-R183W cells, data presented as mean \pm SD
12 (Right) (n=3) (One-way ANOVA; Tukey's correction for multiple comparisons, p-values: ** \leq 0.01, ***
13 \leq 0.001).

14
15 **Figure 5. Expression of R183W decreases sensitivity to MEK Inhibition.** **(A)** Clonogenic assay of M/R
16 cells expressing WT or R183W A α protein. Cells were seeded at 500 cells/well, 24hr after seeding cells
17 were treated with vehicle control or increasing concentrations of AZD-6244 and allowed to grow for 10
18 days. Cells were fixed and stained with crystal violet and quantified using ImageJ. The graph represents the
19 mean colony number \pm SD relative to the vehicle control. Three technical replicates per biological replicate
20 (n=3). (2-Way ANOVA, with Tukey's correction for multiple comparisons, p-values: * < 0.05, **** \leq
21 0.0001). **(B)** Representation of the clonogenic assay as a log dose-response curve, data represented as mean
22 \pm SD (n=3). **(C)** Corresponding graph of the calculated EC₅₀ values for each of the cell lines, data
23 represented as mean \pm SD (n=3). **(D)** 5x10⁶ SW620 cells expressing WT or R183W A α protein or EGFP
24 control vector were injected subcutaneously in nude mice (n=10 per group) and allowed to grow to 100
25 mm³, randomized and treated with 25 mg/kg AZD-6244 BID for 22 days. Graph represents the mean tumor

- 1 volume \pm SEM, (2-Way ANOVA, with Tukey's correction for multiple comparisons, p-values: ** \leq 0.01,
- 2 *** \leq 0.001, EGFP vs. R183W).
- 3

Figure 1

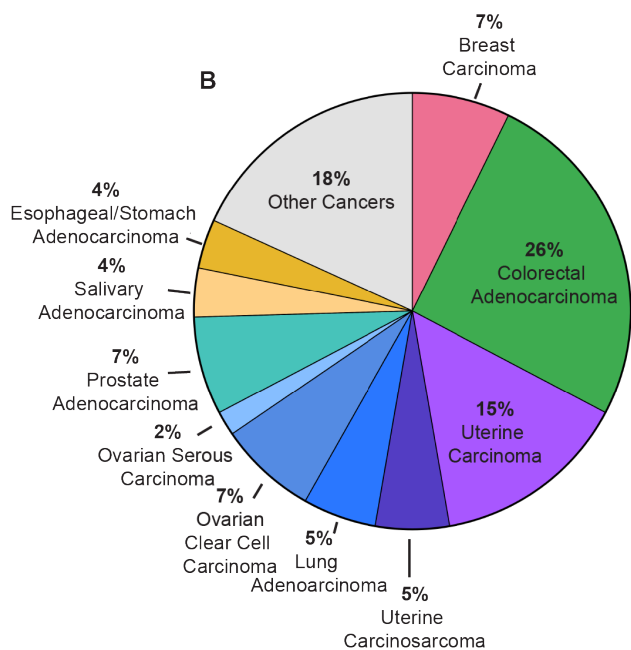
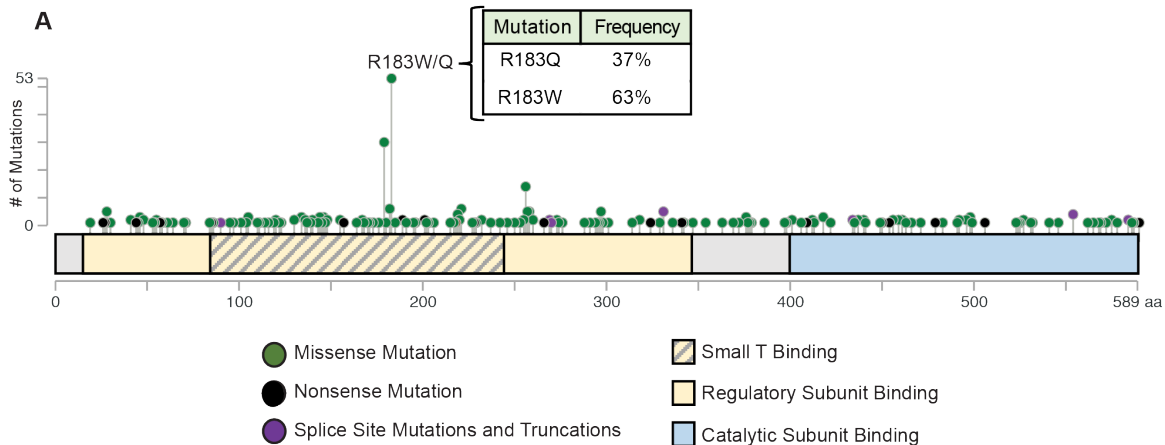


Figure 2

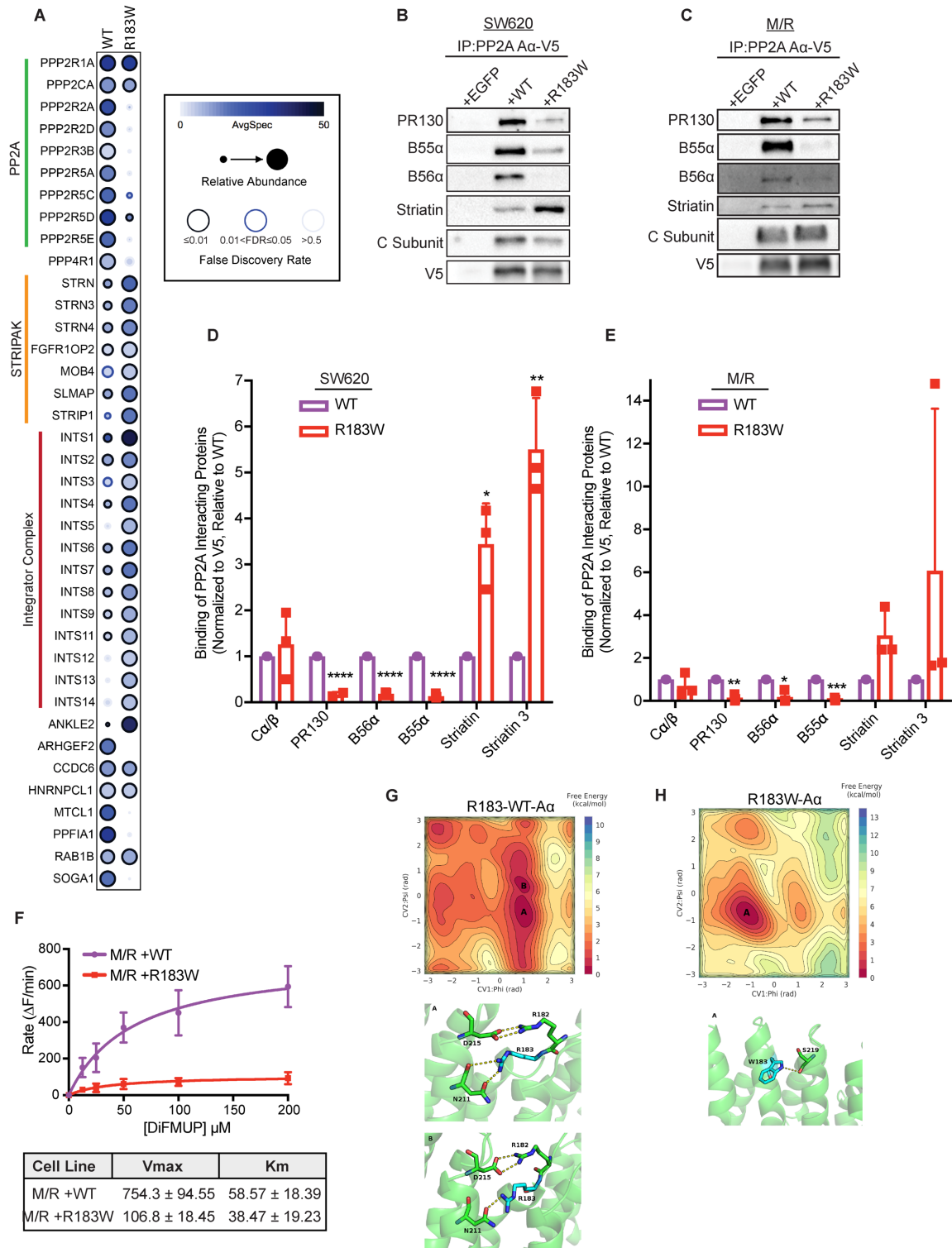


Figure 3

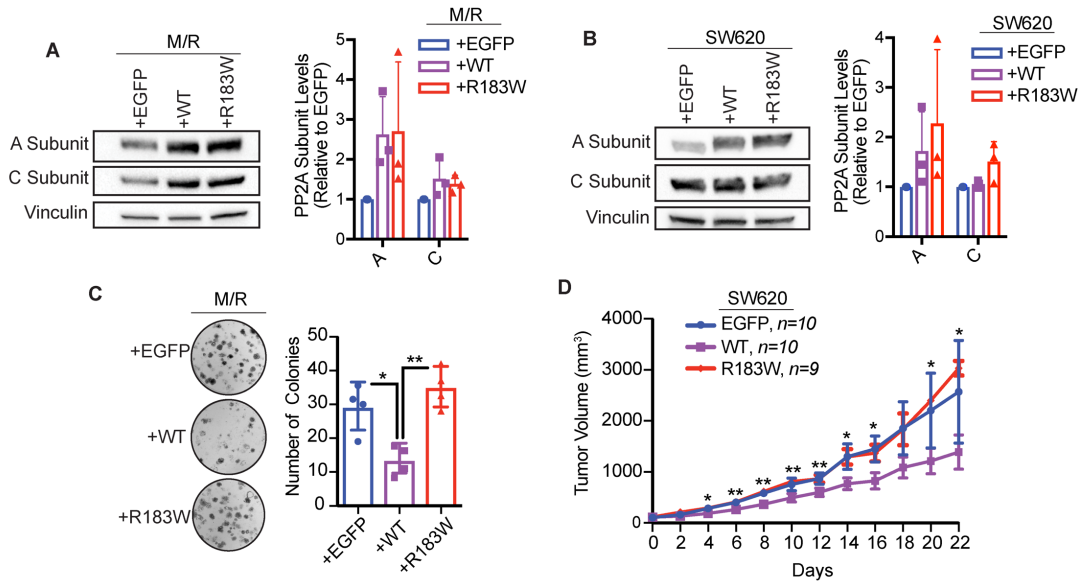


Figure 4

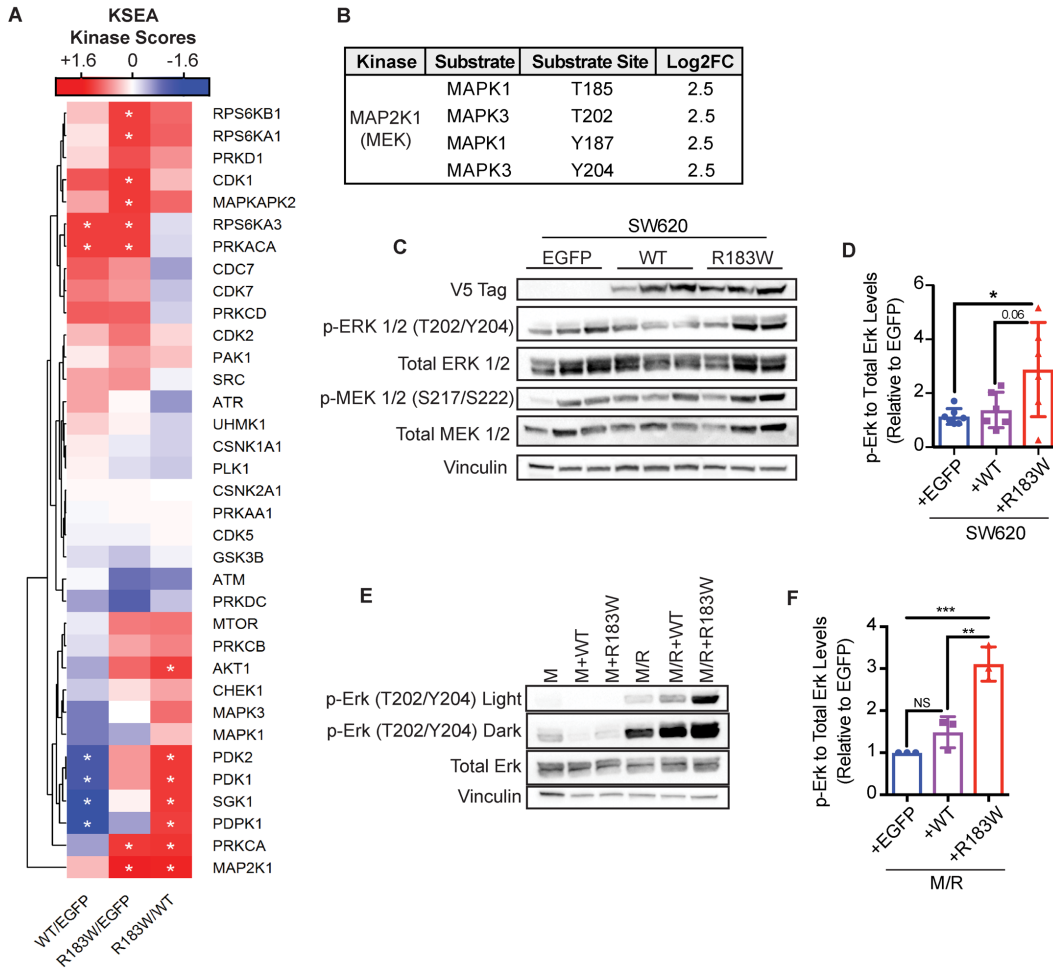
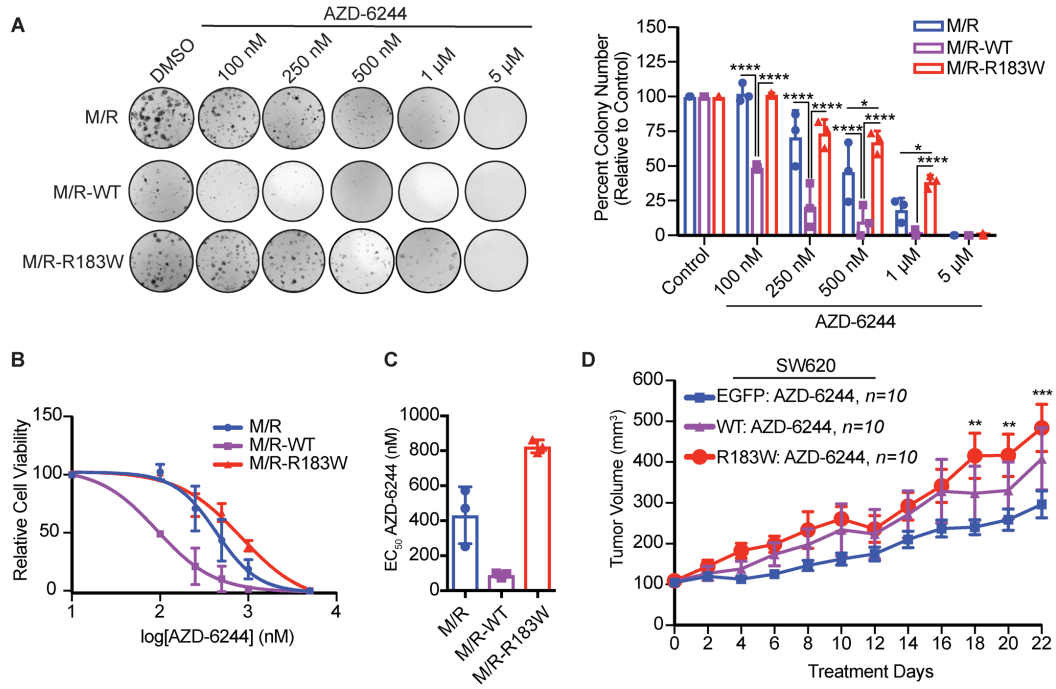
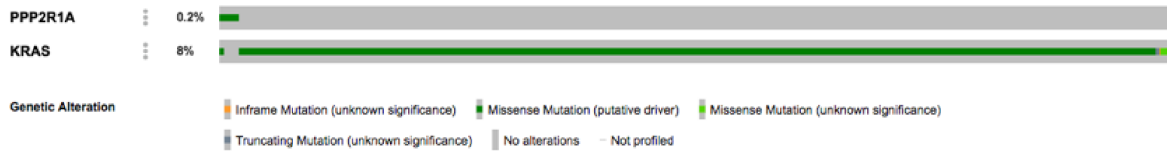


Figure 5



Supplementary Materials

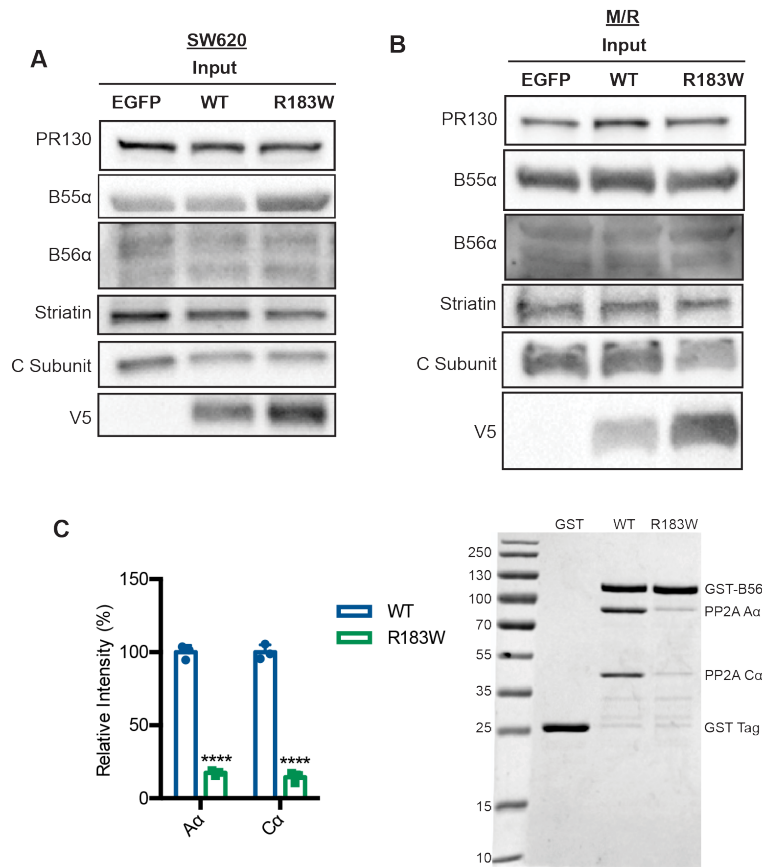
A



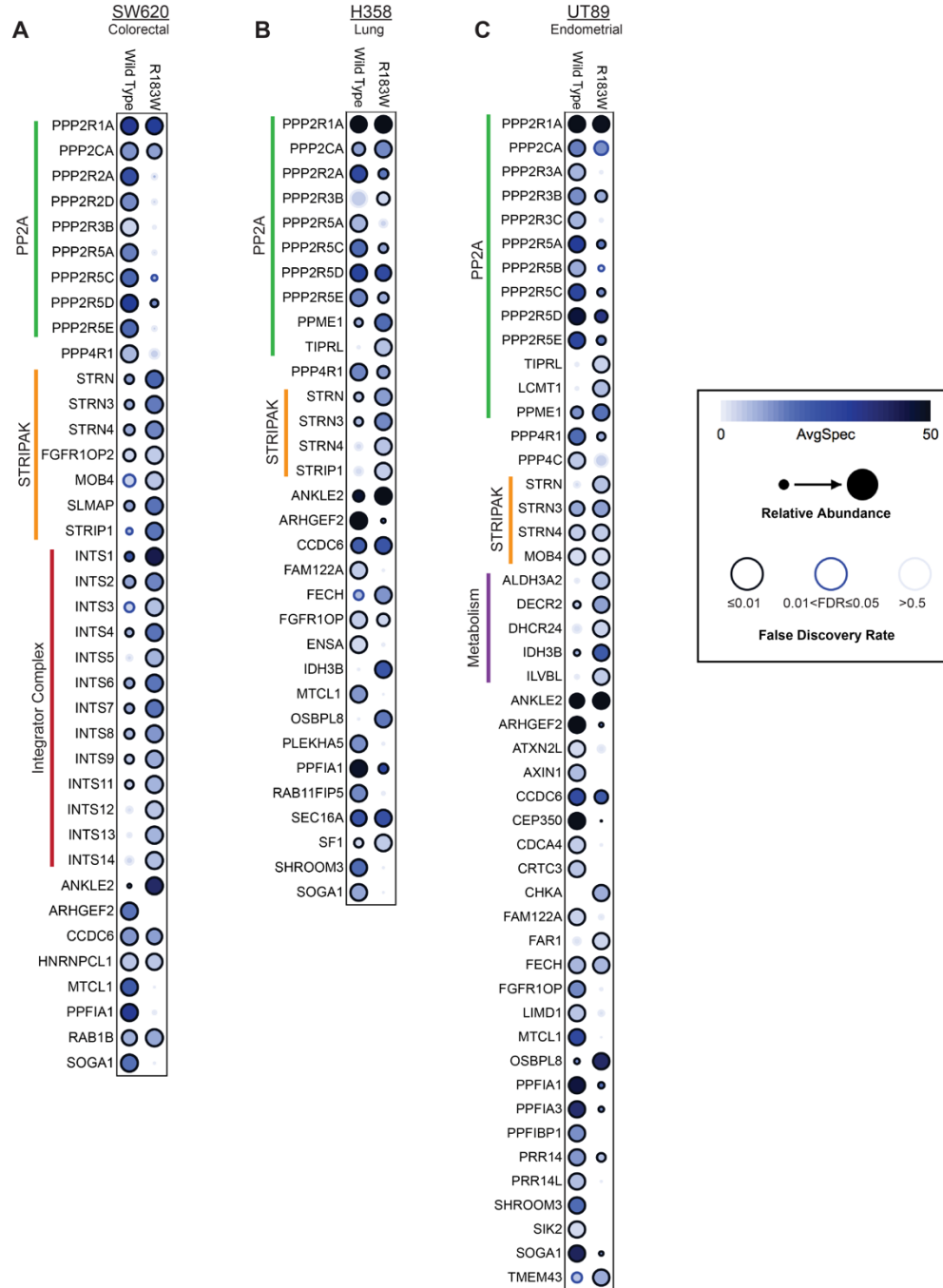
B

Gene A	Gene B	Neither	A Not B	B Not A	Both	Log Odds Ratio	p-Value	Adjusted p-Value ▲	Tendency
PPP2R1A	KRAS	24987	37	2144	10	1.147	0.003	0.003	Co-occurrence Significant

Supplemental Figure 1: R183 Aα mutations co-occur with KRAS mutations. All TCGA datasets, MSK-Impact Study, and TARGET studies accessible through cBioPortal.org were analyzed for R183 Aα mutations and KRAS mutations. **(A)** Oncoprint showing the overall percentage of R183 Aα mutations and KRAS mutations across all cancer. **(B)** Table of mutual exclusivity analysis of R183 mutations and KRAS mutations calculated through cBioPortal.org, showing a significant co-occurrence of R183 mutations and KRAS.

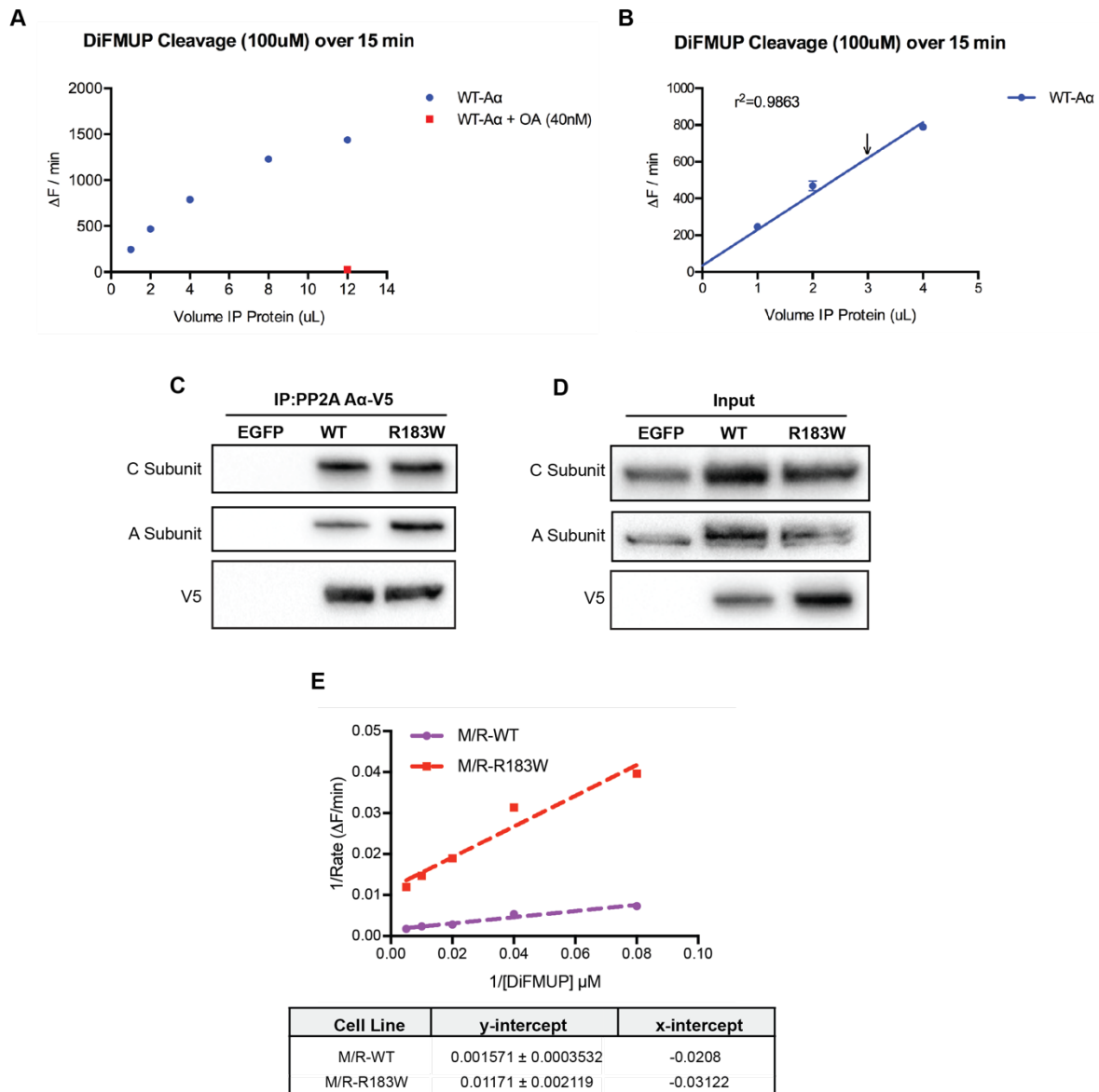


Supplemental Figure 2. Quantification of HMEC and SW620 Co-Immunoprecipitation Experiments. (A and B) Representative Western blots of input samples from co-immunoprecipitation experiments in SW620 (A) and M/R cells (B) related to Figure 2. (C) *In vitro* pull-down assay with GST-tagged B56α conjugated to beads. Recombinant WT or mutant R183W AC dimer was incubated with the beads and allowed to complex with B56α. The resulting complexes were washed off and the eluate was run on a SDS-PAGE gel and stained with coomassie, data presented as the mean ± SD (n=3) (Unpaired two tailed T-test, ****<0.0001).



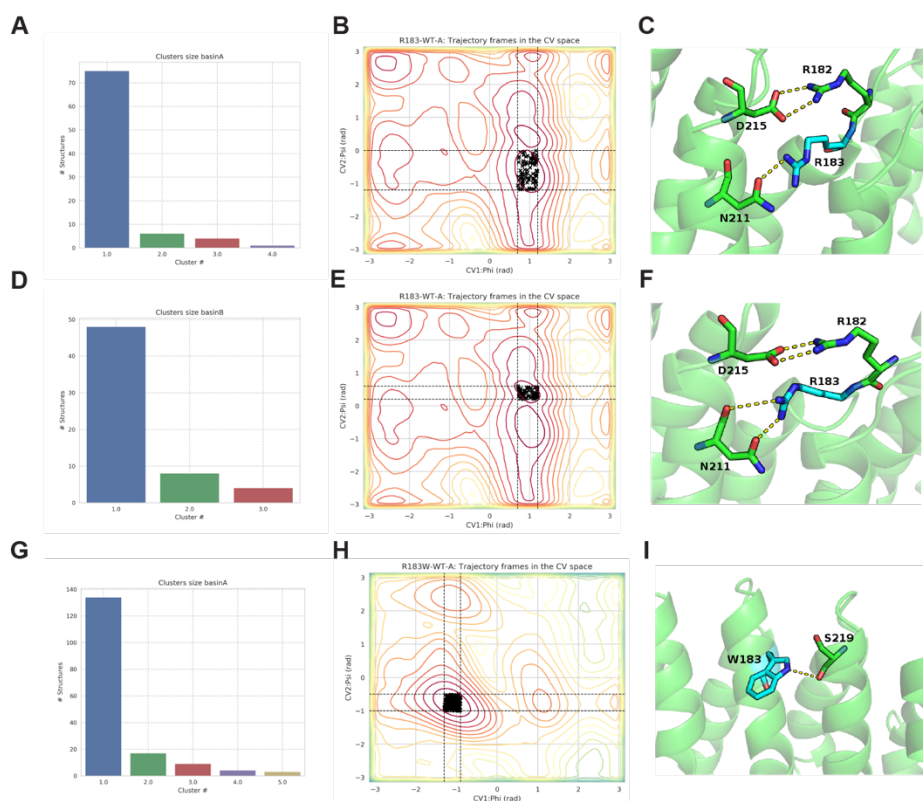
Supplemental Figure 3. AP-MS of R183W across multiple cell lines. (A-C) Affinity purification Mass-Spec (AP-MS) analysis of V5-tagged wild type or R183W α protein from SW620 cells (A), H358 cells (B) and UT89 cells (C). Briefly, V5-tagged WT or R183W α protein and V5-tagged EGFP (control) was expressed in SW620, H358 and OV89 cells. Co-immunoprecipitation analysis was performed by using V5 conjugated beads. After co-immunoprecipitation of complexes, samples were sent for mass spec analysis.

Statistical analysis to determine true interactors was performed by Significance Analysis of INTERactome (SAINT) through the online Contaminant Repository of Affinity Purification (CRAPome) interface at crapome.org. The V5-EGFP interactome as a negative control group. Visualization of protein networks was performed using ProHits-viz using the Dot Plot generator at prohits-viz.lunenfeld.ca, (n=3 for each cell line). Functional classification of select protein groups is highlighted on the left of each dot plot.



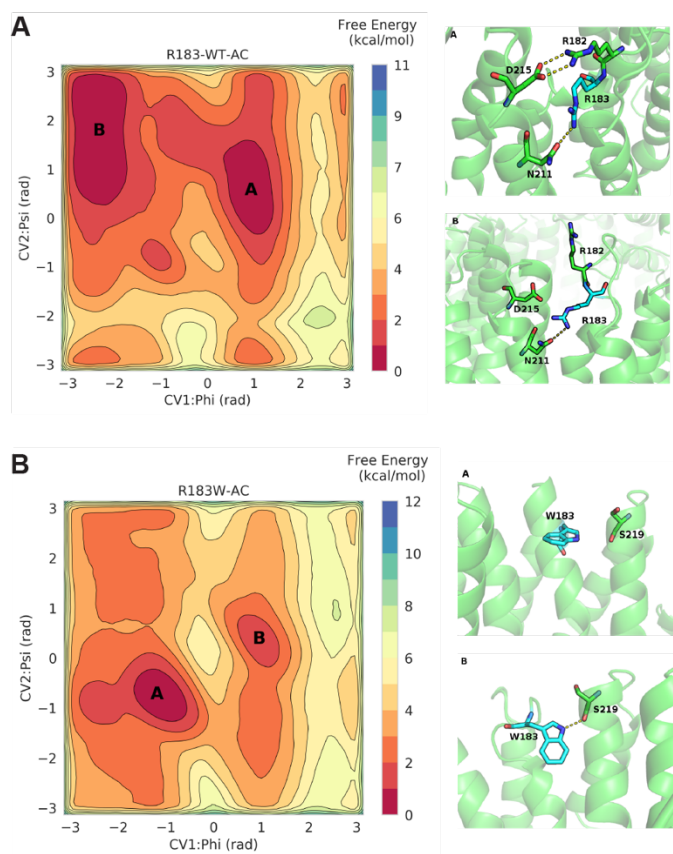
Supplemental Figure 4. Phosphatase activity of co-immunoprecipitated WT and R183W Aα holoenzymes. (A) Establishment of the linear range of phosphatase activity by co-immunoprecipitated PP2A. Briefly, V5-tagged Aα was co-immunoprecipitated and increasing volumes of the resulting lysate were incubated with 100 μM of DiFMUP for 15 minutes and analyzed for activity by fluorescence. The rate of cleavages per minute at each IP volume was graphed (n=2). (B) The linear range of co-immunoprecipitated lysates (n=2). Arrow indicates 3 μL of co-immunoprecipitated Aα lysate, which is within the linear range of the assay and the volume of co-immunoprecipitated lysate used for subsequent assays. (C) Representative Western blot of total A and C subunit levels of the M/R-EGFP, M/R-WT and M/R-R183W CoIP lysate used for phosphatase activity (Figure 2D). (D) Representative Western blot of total A and C subunit levels from the whole M/R-EGFP, M/R-WT and M/R-R183W cell lysate prior to co-

immunoprecipitation and phosphatase activity (Figure 2D). **(E)** Double reciprocal plot of the phosphatase activity of co-immunoprecipitated A α WT and R183W protein (n=3). Calculated x-intercepts ($1/[DiFMUP]$) and y-intercepts ($1/V_{max}$). Mutation to R183W had no change on the x-intercept, indicating no change in K_m , while the y-intercept was increased, indicating decreased V_{max} .

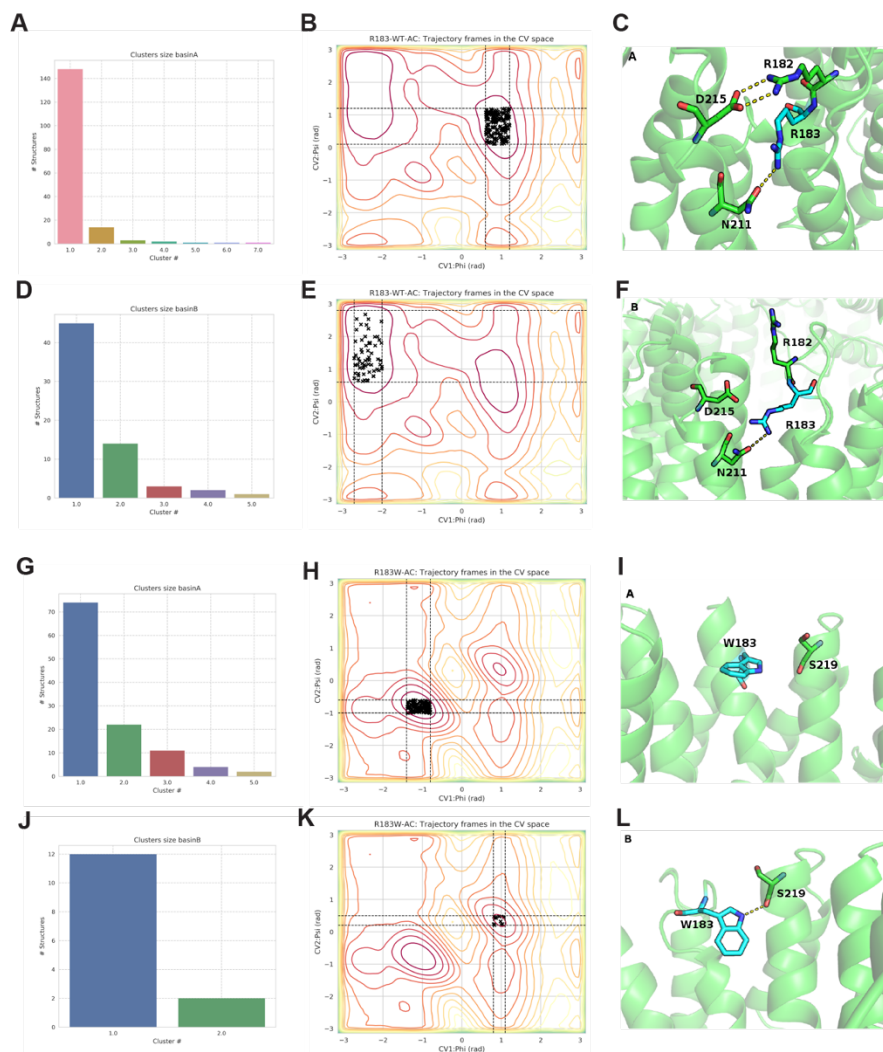


Supplemental Figure 5. WT A α subunit (A-F): (A) Clusters identified based on an RMSD cutoff 3.5Å in the minima A. In total, 4 clusters were identified. (B) Free energy surface (FES) plot calculated from Well Tempered-metadynamics simulations. The energy minima from which the representative structures were extracted for clustering are highlighted in black cross. (C) The representative structure of the clustered conformations in the minima has been illustrated. In this conformation, the side chain of R183 makes interactions with the side chain of N211. This interaction is facilitated by an ion pair interaction between R182 and D215. (D) Clusters identified based on an RMSD cutoff 3.5Å in minima B. In total, 3 clusters were identified. (E) Free energy surface (FES) plot calculated from Well Tempered-metadynamics simulations. The energy minima from which the representative structures were extracted for clustering are highlighted in black cross. (F) Interactions between N211 and R183 and R182 and D215 in the representative structure. Here, the side chain of R183 makes interactions with the side chain of N211. This interaction is facilitated by an ion pair interaction between R182 and D215. R183W A α subunit (G-I): (G) Clusters identified based on an RMSD cutoff 3.5Å in minima A. In total, 5 clusters were identified. (H) Free energy surface (FES) plot calculated from Well Tempered-metadynamics simulations. The energy minima from which the representative structure was extracted for clustering are highlighted in black cross.

(I) The R183W representative structure of the clustered conformations in the minima has been illustrated. Here, the side chain of W183 makes interactions with the side chain of S219.



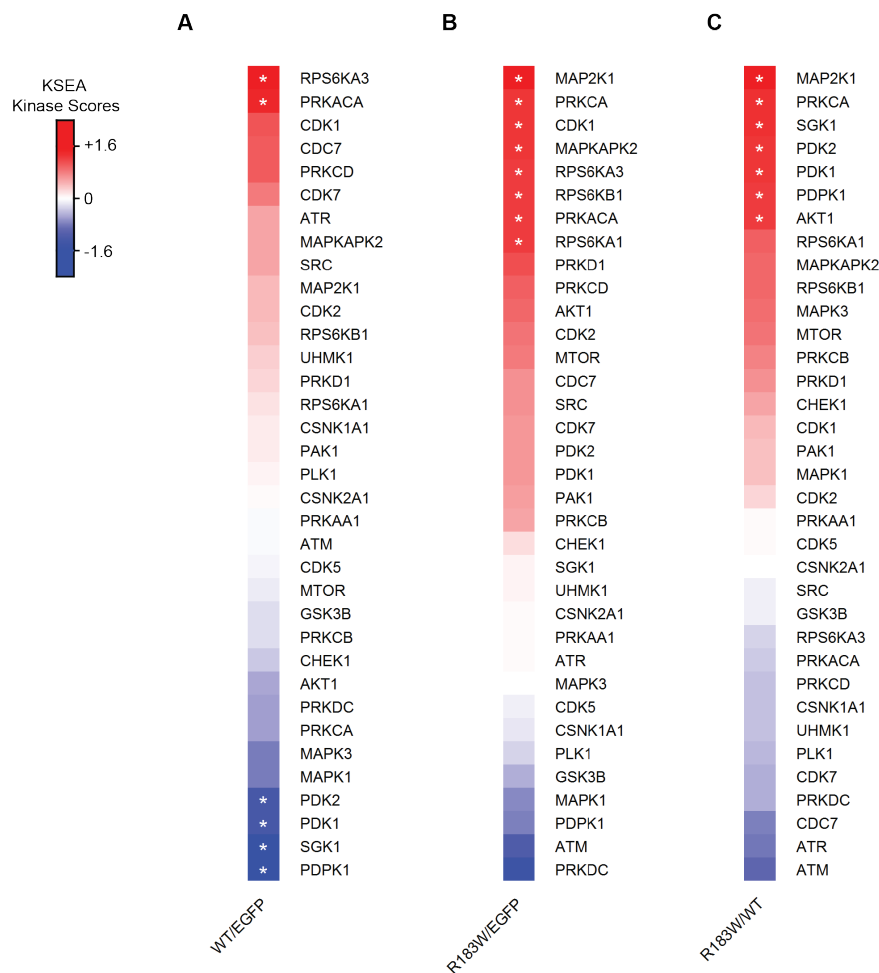
Supplemental Figure 6: Free energy surface conformations of WT and R183W A/C Dimers. (A) Free energy surface (FES) plot of the WT A α + C subunit, as calculated from Well Tempered-metadynamics simulations. The two minima have been labelled as A and B. The representative structure of the clustered conformations in the minima has been illustrated. In the minimum A, the side chain of R183 makes interactions with the side chain of N211. This interaction is facilitated by an ion pair interaction between R182 and D215. In minimum B, the ion pair D215-R182 is broken, while R183-N211 interaction is maintained. **(B)** Free energy surface (FES) plot of the R183W mutant A α + C subunit, as calculated from Well Tempered-metadynamics simulations. The deepest minima have been labelled as A and B. The representative structure of the clustered conformations in the minima has been illustrated. In minima A, there are no interactions between the side chain of R183W mutant and the backbone carbonyl oxygen atom of S219. In minima B, the indole nitrogen makes interactions with the backbone carbonyl oxygen of S219.



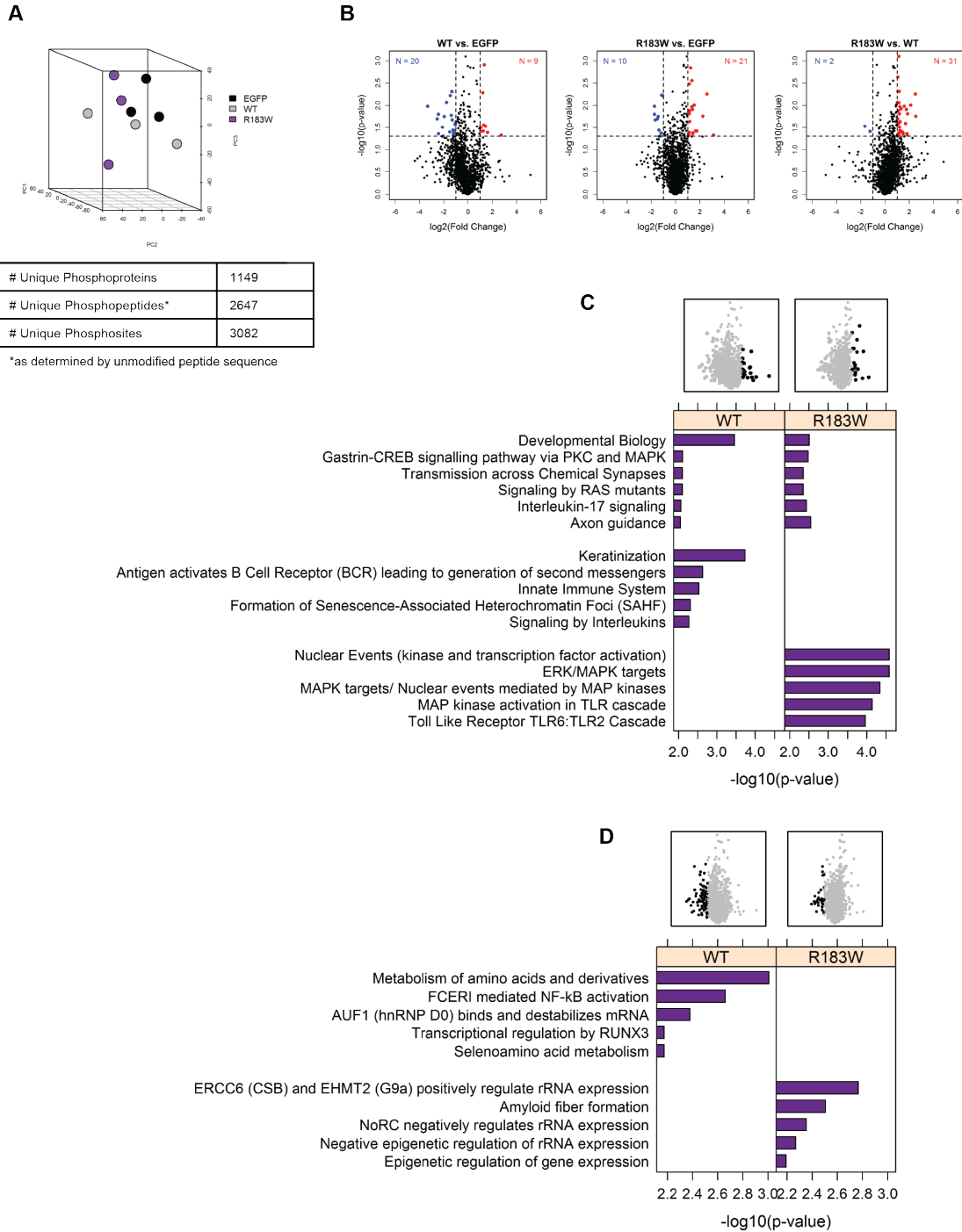
Supplemental Figure 7: WT A α + C Subunit (A-F): (A) Clusters identified based on an RMSD cutoff 3.5Å in the minima A. In total, 4 clusters were identified. (B) Free energy surface (FES) plot calculated from Well Tempered-metadynamics simulations. The energy minima from which the representative structures were extracted for clustering are highlighted in black cross. (C) Interactions between N211 and R183 and R182 and D215 in the representative structure. The representative structure of the clustered conformations in the minima has been illustrated. In the conformation, the side chain of R183 makes interactions with the side chain of N211. This interaction is facilitated by an ion pair interaction between R182 and D215. (D) Clusters identified based on an RMSD cutoff 3.5Å in minima B. In total, 5 clusters were identified. (E) Free energy surface (FES) plot calculated from Well Tempered-metadynamics simulations. The energy minima from which the representative structures were extracted for clustering are highlighted in black cross. (F) Interactions between N211 and R183 in the representative structure. The representative structure of the clustered conformations in the minima has been illustrated. In the

conformation, the side chain of R183 makes interactions with the side chain of N211. The interaction between R182 and D215 is lost.

R183W A α + C subunit **(G-L)**: **(G)** Clusters identified based on an RMSD cutoff 3.5Å in minima A. In total, 5 clusters were identified. **(H)** Free energy surface (FES) plot calculated from Well Tempered-metadynamics simulations. The energy minima from which the representative structure was extracted for clustering are highlighted in black cross. **(I)** The R183W representative structure of the clustered conformations in minima A has been illustrated. In the minimum, there is no interaction between the side chain of W183 and the backbone of S219. **(J)** Clusters identified based on an RMSD cutoff 3.5Å in minima B. In total, 2 clusters were identified. **(K)** Free energy surface (FES) plot calculated from Well Tempered-metadynamics simulations. The energy minima from which the representative structure was extracted for clustering are highlighted in black cross. **(L)** The R183W representative structure of the clustered conformations in minima B has been illustrated. In the minimum, the side chain of W183 makes interactions with the backbone of S219.

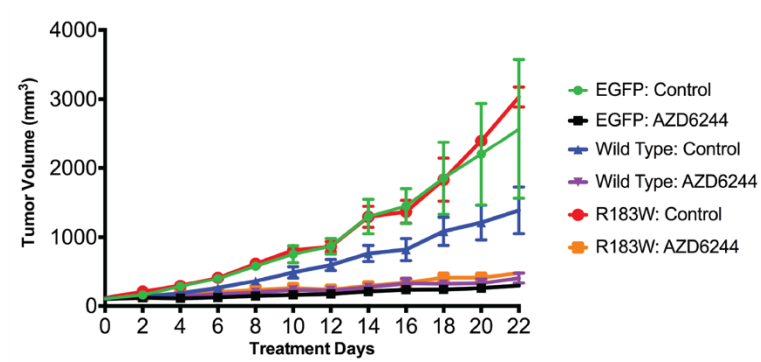
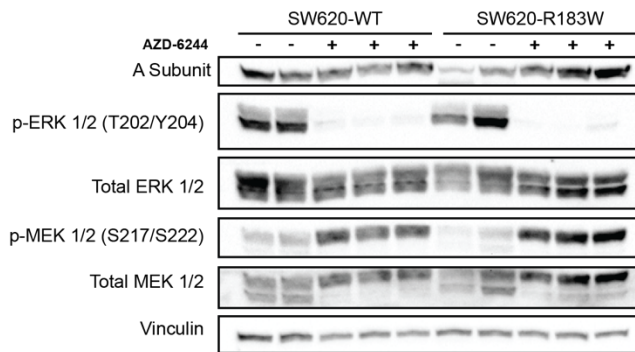


Supplemental Figure 8. Phosphoproteomic kinase level activity analysis (KSEA). (A-C) Kinase-Substrate Enrichment Analysis (KSEA) was performed on the phosphoproteomic dataset to estimate relative changes in kinase activity. The relative changes were determined for the comparisons WT/EGFP (A), R183W/EGFP (B), and R183W/WT (C). The normalized kinase scores are color coded in the heat map; blue = negative score, meaning a decrease in kinase activity in the experimental group (numerator of the fold change) relative to the reference group (denominator). Inversely, red = positive score, which is an increase in kinase activity in the experimental group (numerator) relative to the reference (denominator). White = zero, no change between the groups. Asterisks mark the scores with p-value < 0.05, as calculated by a z-test.

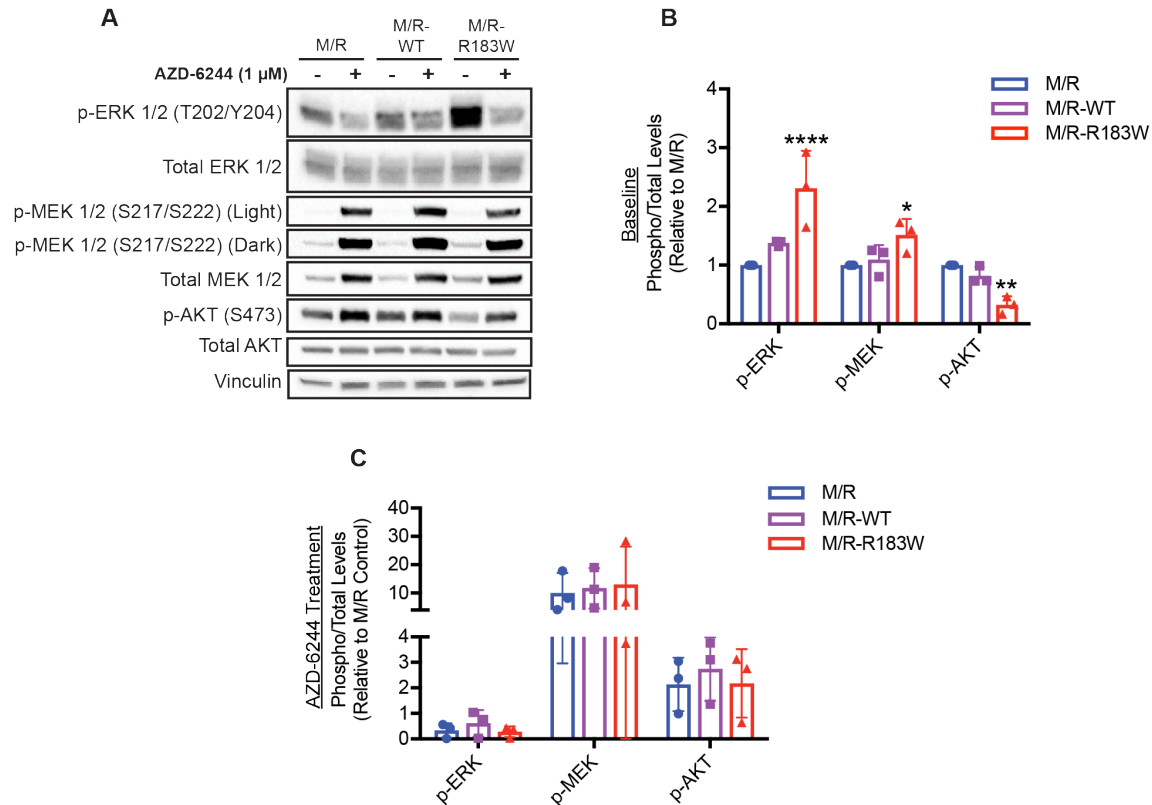


Supplemental Figure 9. Pathway Analysis of SW620 Xenograft shows upregulation of ERK and MAPK targets in R183W expressing tumors. (A) PCA and correlations were used to assess the quality of separation amongst different groups and consistency within a group. PCA plot showed that the samples do not neatly separate according to condition. (B) Volcano plots were generated at the phosphoprotein level. Each dot represents a unique phosphoprotein, whose x and y-axis values were determined from the most

significant peptide. P-values were calculated from a one-way ANOVA across all 3 conditions and are consistent amongst all plots. Fold change (FC) was derived from the ratio of the mean peptide intensity of the peptide in the first group listed in each plot's title, divided by that of the second group. Blue and red dots indicate proteins with $P < 0.05$ + either $\log_2FC \leq -1$ (for blue) or $\log_2FC \geq +1$ (for red). **(C)** Pathway enrichment against the Reactome database was calculated for the proteins meeting $\log_2FC \geq 1.5$ (black dots on mini volcano plot). All shared statistically significant pathways ($p < 0.01$) are listed in this plot; only top 5 pathways unique to each group are included for brevity. P-values were calculated from Fisher's exact test (one-sided). Fold change was calculated relative to EGFP. Pathways with no visible bars were not enriched in the indicated condition. **(D)** Pathway enrichment against the Reactome database was calculated for the proteins meeting $\log_2FC \leq -1.5$ (black dots on mini volcano plot). There were no shared pathways that are statistically significant ($p < 0.01$) between the 2 conditions; only top 5 pathways unique to each group are included for brevity. P-values were calculated from Fisher's exact test (one-sided). Fold change was calculated relative to EGFP. Pathways with no visible bars were not enriched in the indicated condition.

A**B**

Supplemental Figure 10. SW620 AZD-6244 Treated Xenograft. (A) Xenograft assay of SW620 cells expressing EGFP (control vector), wild type A α or A α -R183W, injected subcutaneously into the flanks of nude mice. Tumors were measured every other day, minimum of 9 animals per group. Once tumors reached 100 mm³ animals were randomized into vehicle control or AZD-6244 (25mg/kg BID) treatment groups. Graph represents the mean tumor volume \pm SEM. (B) Representative Western blot of phosphorylated levels of control and AZD-6244 treated WT and R183W expressing SW620 tumors. Briefly, 2 hours prior to sacrifice animals were given the last treatment dose before tumor tissue was collected. The tumor lysate was analyzed for phosphorylated and total levels of MEK and ERK, as well as total A subunit, and Vinculin levels.



Supplemental Figure 11. Phosphorylation levels of MAPK and AKT pathway proteins at baseline and upon MEK inhibition. (A) Representative western blot of M/R, M/R-WT, and M/R-R183W cells treated with DMSO or 1 μ M AZD-6244 for 24 hours, (n=3). (B) Quantification of baseline phosphorylation levels of ERK, MEK, and AKT in M/R, M/R-WT, and M/R-R183W cells. Phosphorylation levels were quantified by a ratio over total protein and graphed relative to the phospho/total ratio in M/R cells, data presented as the mean \pm SD (n=3). (2-way ANOVA of M/R WT and M/R-R183W compared to M/R control cells, Dunnett's multiple comparison test, * <0.05 , ** <0.01 , *** <0.001 , **** <0.0001). (C) Quantification of phosphorylation changes in M/R, M/R-WT, and M/R-R183W cells in response to AZD-6244 treatment. Phosphorylation levels were quantified by a ratio over total protein and graphed relative to the baseline phosphor/total ratio in M/R cells, data presented as the mean \pm SD (n=3). (2-way ANOVA of M/R WT and M/R-R183W compared to M/R control cells, Dunnett's multiple comparison test).

Table S1: KRAS and MSI Status of R183 mutant CRC patients

Sample	Study	Codon	KRAS Status	MSI Status	# of Mutations in Sample
dfci_2016_4538		R183Q	Q61K (NRas)	MSS	305
dfci_2016_3105		R183Q	WT	MSS (Stage III)	81
dfci_2016_180077	Colorectal DCFI (2016)	R183Q	WT	Stage III**	112
dfci_2016_3422		R183W	WT	MSI-H (Stage II)	664
dfci_2016_2430		R183W	G12D	MSS (Stage III)	175
dfci_2016_160282		R183W	G12C & G12V	Stage II**	127
TCGA-AA-3514-01		R183W	WT	MSS (Stage I)	60
TCGA-AA-3846-01	Colorectal TCGA	R183W	WT	MSS (Stage IIA)	69
TCGA-AA-A01R-01		R183W	G13D	MSI-H (Stage III)	1226
P-0001769-T01-IM3			R183W	G12D	N/A**
P-0002788-T01-IM3		R183W	G12D	N/A**	14*
P-0006207-T01-IM5	MSK-IMPACT*	R183W	Q61K	N/A**	59*
P-0008180-T01-IM5		R183W	WT	N/A**	76*
P-0011239-T02-IM5		R183W	G12R	N/A**	84*

*Targeted sequencing of a 468 gene oncopanel

**MSI Status Not Reported

Table S2: Antibodies used in this study

Antibody	Source	Catalogue Number
PP2A A Subunit	Cell Signaling	2041S
PP2A C Subunit	Abcam	ab106262
Striatin	Sigma	PA146460
Striatin 3	Sigma	MA146461
B56 α	Abcam	ab89621
B55 α	Santa Cruz	sc-18606
PR130/PR72	Thermo-Fisher	PA5-30127
ERK	Cell Signaling	9102L
p-ERK (T202/Y204)	Cell Signaling	4370L
AKT	Cell Signaling	9279S
p-AKT (S473)	Cell Signaling	4060L
MEK	Cell Signaling	9126S
p-MEK (S217/221)	Cell Signaling	9154S
Vinculin	Cell Signaling	13901S
V5 (Western Blot)	Cell Signaling	13202S
V5 (CoIP)	Abcam	ab27671